UNIVERSITY OF CALIFORNIA SAN DIEGO

Advanced Right Ventricular Functional Analysis in End-Stage Heart Failure with CT

A Dissertation submitted in partial satisfaction of the requirements
for the degree Doctor of Philosophy

in

Bioengineering

by

Anderson Royal Scott

Committee in charge:

Professor Francisco Contijoch, Chair
Professor Seth Kligerman
Professor Andrew McCulloch
Professor Elliot McVeigh
Professor Farah Sheikh

2023

The Dissertation of Anderson Royal Scott is approved, and it is acceptable in quality and form for publication on microfilm and electronically.

University of California San Diego

2023

DEDICATION

To my parents, my siblings Berrimond, Lewis, and Anna, and my loving partner, Josh. I'm lucky to call them family.

TABLE OF CONTENTS

LIST OF FIGURES

LIST OF TABLES

LIST OF ABBREVIATIONS

AUC	Area Under the Curve
AST	Aspartate Transaminase
BiVAD	Biventricular Assist Device
BMI	Body Mass Index
BSA	Body Surface Area
BUN	Blood Urea Nitrogen
CI	Cardiac Index
CO	Cardiac Output
CT	Computed Tomography
EDPVR	End Diastolic Pressure Volume Relationship
EDVI	End Diastolic Volume Index
EF	Ejection Fraction
ESVI	End Systolic Volume Index
ESPVR	End Systolic Pressure Volume Relationship
EUROMACS	European Registry for Mechanically Assisted Circulatory Support
FW	Free Wall
GFR	Glomerular Filtration Rate
HF	Heart Failure
HFpEF	Heart Failure with preserved Ejection Fraction
HR	Heart Rate
ICD	Intracardiac Device
INR	Internal Normalized Ratio

INTERMACS	International Registry for Mechanically Assisted Circulatory Support
LV	Left Ventricular
LVAD	Left Ventricular Assist Device
MPAP	Mean Pulmonary Arterial Pressure
MRI	Magnetic Resonance Imaging
PAd	Pulmonary Arterial Pressure, Diastole
PAPI	Pulmonary Arterial Pulsatility Index
PAs	Pulmonary Arterial Pressure, Systolic
PCWP	Pulmonary Capillary Wedge Pressure
PV	Pressure-Volume
PVA	Pressure-Volume Area
PVR	Pulmonary Vascular Resistance
RAP	Right Atrial Pressure
RHC	Right Heart Catheterization
ROC	Receiver Operating Characteristic
RR	R-to-R Interval (Cardiac Cycle)
RV	Right Ventricular
RVAD	Right Ventricular Assist Device
RVF	Right Ventricular Failure
RVPP	Right Ventricle Pulse Pressure
RVSWI	Right Ventricular Stroke Work Index
SQUEEZ	Stretch Quantification of Endocardial Engraved Zones
SV	Stroke Volume

SVI	Stroke Volume Index
SW	Septal Wall
TAPSE	Tricuspid Annular Plane Systolic Excursion
TR	Tricuspid Regurgitation
WBC	White Blood Cell Count

ACKNOWLEDGEMENTS

First and foremost, I would like to thank my advisor, Francisco Contijoch, for his mentorship and support. When I first joined his lab, he and I were the only members. Since that time, the lab has had immense growth and success, which can only be seen as a testament to his leadership. Similarly, through his guidance, I have felt myself grow from a student with an interest in cardiology into an expert in analyzing right ventricular dysfunction in heart failure. He has helped me become even more confident and capable as a researcher than I could have imagined. For this, I will always be grateful.

Thank you to the members of my dissertation committee for sharing resources and providing insight that have been crucial to my projects.

I would also like to thank the heart failure team at UCSD. They have aided me in understanding much of the clinical data and allowed me to see how these tools may be used for patient care. Specifically, I would like to thank Drs Seth Kligerman, Paul Kim, Hao Tran, Victor Pretorius, and Eric Adler for providing insight and help with drafting the manuscripts which went on to be the core chapters of this dissertation.

I'm grateful to the entire Contijoch Research Lab and Cardiovascular Imaging Lab. They invited me into a research setting that was fun, collaborative, and focused. They sent me papers, read through my drafts, and provided a sense of community. My PhD experience would not have been half as enjoyable without them.

Chapter 1, in full, is a reprint of the material as it appears as "Preoperative Computed Tomography Assessment of Risk of Right Ventricle Failure After Left Ventricular Assist Device Placement" in the *American Society for Artificial Internal*

Organs, 2022 by Anderson Scott, Seth Kligerman, Diana Hernandez Hernandez, Paul Kim, Hao Tran, Victor Pretorius, Eric Adler, and Fracisco Contijoch. The dissertation author was the primary investigator and author of this paper.

Chapter 2, in part, is a reprint of the material as it appears as "Pressure Volume Loop Analysis of the Right Ventricle with Computed Tomography in Heart Failure" in the *American Society for Artificial Internal Organs*, 2022 by Anderson Scott, Zhennong Chen, Diana Hernandez Hernandez, Seth Kligerman, Paul Kim, Hao Tran, Eric Adler, and Francisco Contijoch. The dissertation author was the primary investigator and author of this paper.

Chapter 3, in part, is currently being prepared for submission for publication of the material as it appears as "Free and Septal Wall Function for Risk Assessment in Heart Failure using Computed Tomography" by Anderson Scott, Zhennong Chen, Seth Kligerman, Paul Kim, Hao Tran, Eric Adler, and Francisco Contijoch. The dissertation author is the primary investigator and author of this manuscript.

VITA

2016 Bachelor of Engineering in Biomedical Engineering, Virginia Commonwealth University

2023 Doctor of Philosophy in Bioengineering, University of California San Diego

PUBLICATIONS

Scott A, Kligerman S, Hernandez Hernandez D, Kim P, Tran H, Pretorius V, Adler E, Contijoch F. Preoperative Computed Tomography Assessment of Risk of Right Ventricle Failure After Left Ventricular Assist Device Placement. *ASAIO*. 2022. DOI:10.1097/ MAT.0000000000001710

Scott A, Chen Z, Hernandez Hernandez D, Kligerman S, Kim P, Tran H, Adler E, Contijoch F. Pressure Volume Loop Analysis of the Right Ventricle with Computed Tomography in Heart Failure. *ASAIO*. DOI: 10.1097/MAT.0000000000001869.

Gupta K, Sekhar N, Vigneault D, **Scott A**, Colvert B, Craine A, Raghavan A, Contijoch F. Octree Representation Improves Data Fidelity of Cardiac CT Images and Convolutional Neural Network Semantic Segmentation of Left Atrial and Ventricular Chambers. Radiology: AI. 2021. DOI:10.1148/ryai.2021210036

ABSTRACT OF THE DISSERTATION

Advanced Right Ventricular Functional Analysis in End-Stage Heart Failure with CT

by

Anderson Royal Scott

Doctor of Philosophy in Bioengineering

University of California San Diego, 2023

Professor Francisco Contijoch, Chair

For patients in advanced stages of heart failure, a left ventricular assist device (LVAD) may be surgically implanted to aid in systemic circulation, either as a bridge to heart transplant or as a destination therapy. As such, LVAD implantations have become a standard for patient care for end-stage heart failure patients who are unable to receive a heart transplant. A major complication, however, is the postoperative adverse event of

right ventricular failure (RVF). RVF occurs in approximately 10-40% of all patients undergoing LVAD implantation and has been linked to longer length of stay in intensive care unit, lower quality of life, and higher mortality. As such, there is a critical need to identify patients who are at a high risk for RVF prior to implantation to optimize patient care. Previous studies have attempted to assess risk using risk scores based on hemodynamics, patient characteristics, and disease presentation, but have found limited predictive potential. A major limitation of these previous studies is the difficulty to characterize pre-operative right ventricular function quantitatively. CT is uniquely able to aide in quantitative RV analysis as it provides clinicians with 3D volumetric data and visualizations of localized function throughout the cardiac cycle. Additionally, CT data can be combined with hemodynamic data for advanced RV measures that have never been analyzed in this clinical setting. Despite this potential, CT has seen very limited use to analyze preoperative RV function in this patient population. The focus of this work is to use pre-LVAD CT imaging to create tools that improve preoperative RV assessment to assess RVF risk. To do this, we investigate (1) the ability of CT-derived volumetry to characterize global function and identify RV dysfunction. We then examined (2) the ability of combined volumetric and hemodynamic data to measure RV energetics. Finally, we use CT to investigate (3) the ability of regional RV function in the context of CT-based volumetry and hemodynamic data to identify RV dysfunction and identify markers of high-risk patients.

INTRODUCTION

Heart Failure and Left Ventricular Assist Devices (LVADs)

Heart failure affects approximately 26 million patients worldwide and represents a significant cause of mortality[1]. In the United States, an estimated 1-3% of adults are living with heart failure[2]. Heart failure patients are classified by left ventricular ejection fraction (ratio of ejected volume to volume at end diastole) with their own distinct phenotypes. Patients with an ejection fraction less than 40% have heart failure with reduced ejection fraction (HFrEF) while those with greater than 40% ejection fraction have heart failure with preserved ejection fraction (HFpEF). Patients with HFpEF are often older (over 80), female (>70%), and have higher rates of atrial fibrillation and hypertension[3]. Patients with HFrEF are more commonly male (>70%) with a history of myocardial infarction[4, 5]. For patients with acute heart failure, the gold standard treatment is a heart transplant; however, due to the scarcity of heart transplants, the use of mechanical circulatory support in the form of left ventricular assist devices (LVADs) has grown significantly, particularly as a means of prolonging life until a transplant becomes available. This is often referred to as a bridge to transplantation (BTT) mechanical support. Due to the decreased cavity size and increased myocardium thickness in HFpEF, LVAD therapy targets HFrEF patients[6].

The patients referred for LVAD implantation are a small subset of patients with an advanced stage of heart failure such that they experience clinical worsening despite optimal medical therapy. In order to analyze post operative trends in this population, many databases have been created. The Interagency Registry for Mechanically Assisted Circulatory Support (INTERMACS) was established in the US in 2005[7]. Additional databases include the European Registry for Patients with Mechanical Circulatory Support (EUROMACS)[8], the

Japanese Registry for Mechanically Assisted Circulatory Support (J-MACS)[9], and the UK registry. Data from these registries provide information on the LVAD population along with long-term follow-up data.

Patient outcomes have been affected by changes to LVAD technology. First generation LVADs (HeartMate I, HeartMate VE, and HeartMate XVE) were refined in the 1990s and were pulsatile volume displacement pumps. Second generation LVADs (HeartMate II) were continuous flow, rotary pumps that used continuous axial flow to pull blood through the pump to generate flow. The third generation LVADs (HeartMate III) used centrifugal pumps with a spinning impeller to propel blood and generate forward flow[10]. As pumps become more advanced, mortality rates have dipped, encouraging their greater use though there is still controversy regarding the appropriate time to implant[7]. Categories have been developed to classify heart failure patients based on clinical profile. INTERMACS has 7 clinical profiles that have been used to describe heart failure severity where 1 is the most severe (critical cardiogenic shock) and 7 is the least severe (limited physical ability and comfortable at rest)[11]. Between 2013 and 2017, 16,194 LVADs have been implanted and the proportion of patients fitting INTERMACS profiles 1 through 7 have remained stable each year[12]. The growth of bridge to transplant LVAD implantation has been rapid from 2007 until present but seems to be stabilizing at 45% of LVAD implantations[13].

Quality of life for heart failure patients is often measured using questionnaires, such as the Kansas City Cardiomyopathy Questionnaire (KCCQ), which asks questions regarding activities of daily living, shortness of breath, and edema to score patient wellbeing out of 100 possible points. Generally, scores tend to slightly improve over time for heart failure patients, particularly with the use of exercise and spironolactone compared to control[5]. Following

LVAD implantation, there is an initial drop in quality-of-life indicators, followed by substantial improvements. A study using KCCQ survey data and INTERMACS registry data noted a mean baseline score of 34.6, and scores of 14.3 at 3 months, 28.1 at 6 months, 41.1 at 9 months, and 63.8 at 1 year[14]. For patients who have undergone LVAD implantation, survival is approximately 83% at 1 year[15].

Ultimately, the increase in patients living with heart failure has prompted interest in their medical management and how advanced therapies can affect quality of life and mortality. Since its inception, LVAD support for heart failure has been a powerful tool in the management of acute heart failure due to its positive effects on survival and quality of life. LVAD support will continue to supplement medical management as the mismatch between patients and donor hearts remains.

Right Ventricular Failure

Mechanical circulatory support is an important aspect of patient care in the management of advanced heart failure[16]. Given the improved survival with left ventricular assist devices (LVADs) in patients ineligible for heart transplantation, the use of LVADs has expanded to ameliorate worsening of end-stage heart failure[17]. While LVADs represent the current treatment standard for patients with worsening condition and waiting for a heart transplant[18], one significant driver of postoperative morbidity and mortality is right ventricular failure (RVF) [19],[20].

RVF is most often defined as the need for pharmacological treatment (inotropes and/or pulmonary vasodilators) for greater than 2 weeks after surgery and is estimated to occur in 10-40% of postsurgical patients.[19–21] For patients with more severe forms of RVF, where

unplanned biventricular support is required, 1-year survival drops from over 80% to below 50%.[19] RVF is thought to be due to changes in loading conditions, interventricular septal function, and primary underlying cardiomyopathy[22, 23]. On its own, RVF portends many adverse outcomes such as prolonged intensive care unit stay, poor life quality, reduced survival to transplantation, and early mortality[19, 23, 24]. Due to these concerns, patients who are at a high risk for RVF may benefit from either upfront biventricular assist device or patient optimization to ensure a better postoperative course. Over the last 2 decades, many models and risk scores have been developed in this patient cohort for this reason[25].

Traditional risk prediction

Both systemic review[26] and meta-analysis[27] of the many risk scores that have been developed have shown poor to modest discrimination (C statistic < 0.8). The reason for this poor performance is varied. It is, in part, related to changes in LVAD technologies over the past 2 decades as well as the variability of inotropic use for RVF between studies, and a limitation of hemodynamic, echocardiographic, biochemical, or clinical measures to quantify RV function directly[26, 27]. Namely, RVF is believed to arise from an interplay of RV dysfunction, elevated filling pressures, afterload, or septal shifts that alter RV mechanics during decompression[28].

Despite this, RVF risk assessments do not use quantifiable markers of intrinsic RV function. Rather, preoperative parameters associated with RV dysfunction, such as elevated filling pressures, and broad visual assessments are used. For example, the European Registry for Mechanically Assisted Circulatory Support (EUROMACS) score, the most widely accepted risk score, accounts for direct RV function by grading RV performance as either functional or dysfunctional based on a visual assessment from 2D echocardiography.[29] This qualitative

assessment introduces variability and speaks to the lack of direct, quantitative RV assessment in current analyses.

RV analysis

Historically, assessment of the right ventricle function has lagged behind the left ventricle as it is less muscular, restricted to only pulmonary circulation, and less clearly involved in cardiac diseases such as myocardial ischemia, cardiomyopathy, and valvulopathy[30]. Typically, the right ventricle functions as a pump to move deoxygenated blood through the pulmonary circulation. The right ventricle pumps the same stroke volume as the left ventricle, but with reduced stroke work due to the low resistance of the pulmonary vasculature[31]. Despite this, its correlation with the outcomes of these diseases suggest that is an important contributor to patients' wellbeing in these disease states[26].

The geometry of the right ventricle is complex. The free wall of the right ventricle is thin and compliant by virtue of the Laplace relationship which states that pressure is directly related to wall tension and inversely related to wall thickness. Due to this compliance and anatomical limitations, the right ventricle is highly influenced by the function of the left ventricle. Primarily, this is because the right ventricle is directly connected to the left ventricle through a shared wall (the septum), a shared pericardial space, mutually encircling epicardial fibers, and through direct attachment at the anterior and posterior septum. Additionally, right ventricle stroke volume is matched to left ventricle stroke volume to prevent circulatory or pulmonary edema[32, 33].

Dysfunction in the right ventricle may develop in tandem with left ventricular dysfunction. This may occur through multiple pathways. Left ventricular dysfunction may increase right ventricular afterload by increasing pulmonary venous and by extension pulmonary

arterial pressure[34]. Decreased systolic function of the left ventricle may decrease coronary perfusion to the right ventricle[35]. Septal dysfunction may reduce right ventricular systolic function through cardiac interdependence. Lastly, left ventricular dilation may limit right ventricular diastolic function in a limited pericardial space. Likewise, dysfunction found primarily in the right ventricle may affect left ventricular function by creating pulmonary hypertension or edema. Because of the multiple ways that left ventricular and right ventricular function affect each other, poor right ventricular function in left sided disease may indicate a common final pathway of impending decompensation[31].

Previous studies that have examined the relationship between right ventricular function in left sided disease continually find evidence that right ventricular dysfunction is coupled with poor outcomes[26, 36]. In patients with heart failure, those who died during the 2 year follow up had worse right ventricular ejection fraction (24%) than survivors (42%)[37]. 1-year mortality in patients with low right ventricular ejection fraction (<38%) and low left ventricular ejection fraction (<30%) was 3 times the mortality in patients with low left ventricular ejection fraction alone[38]. In patients with advanced congestive heart failure, right ventricular shortening is a significant, independent associate of survival by multivariate analysis[39].

Despite these investigations, the exact mechanism by which left ventricular dysfunction confers right ventricular dysfunction is still unknown. One limitation of this research is defining an appropriate measurement that captures right ventricular dysfunction[31]. Right ventricular dysfunction is hard to define for many reasons. Primarily, the function of the right ventricle is widely influenced by the function of the left ventricle, as discussed above, meaning that alleviation of left ventricular dysfunction may alleviate right ventricular dysfunction. Additionally, the right ventricle is affected by loading conditions and so unentangling underlying

myocardial function from measures of pulmonary arterial pressure, for example, requires load independent measures[33]. Further, analysis by 2D-imaging may underestimate volumetric assessments because of the right ventricle's complex geometry[40]. Improved analysis of right ventricular function may thus provide more sensitive predictors of outcomes.

Cardiac cineCT provides full 3D visualization of the right ventricle during the cardiac cycle. Cine-CT scanning is a form of high-speed scanning wherein scanners can acquire full visualizations of cardiac anatomy that can image cardiac contractions. This has been made possible using slip ring technology during image acquisition. In order to image the area of interest, an x-tube and an x-ray detector are mounted on a gantry across from each other on the scanner. These pieces then rotate around the area of interest to collect data. Slip rings forgo the use of cables to allow continuous rotation by creating a continuous connection between a brush and the conductive tract of the slip ring. This technology has made cine-CT possible, particularly cardiac imaging which previously suffered from motion artifacts from the cardiac contractions. Cardiac cine scanning is the fast and continuous acquisition, gated by ECG inputs. Cardiac scanning can cover the entire volume of the heart with one axial scan. Because of this, cine CT is uniquely positioned to derive volumetric data of the heart during the cardiac cycle for heart failure patients who have limitations for cardiac imaging with magnetic resonance imaging (MRI) and echocardiography[41]. This provides clinicians with time varying volumetric data over the cardiac cycle as well as complete visualization of the endocardial free and septal wall motion.[42] These parameters, combined with hemodynamic measurements, can provide further opportunities to assess the RV with pressure-volume loop analysis, a reference standard for assessing cardiac parameters.[43] These would provide the direct, quantitative assessments of RV function that are lacking in current RV assessment.

Dissertation Overview

This dissertation is divided into 3 subsequent chapters. Chapter one analyzes the concordance of echocardiographic assessments of volume and function with CT volumetry and ejection fraction. It then compares the predictive potential of CT derived measures of RV volume and ejection fraction to echocardiographic data, hemodynamic data, and patient characteristics in patients that went on to have LVAD implantation. These findings are then used to suggest a possible cutoff volume for severe RV enlargement which would confer some risk of RV failure.

Chapter two then expands on these findings of echocardiography's limitations to examine the most common hemodynamically derived measure of RV function, right ventricular stroke work index (RVSWI). RVSWI is estimated clinically as the product of the stroke volume, which only measures forward flow, and mean pulmonary pressure. This measure is compared to RVSWI derived directly from a pressure-volume loop created from contemporaneous CT volumetric data and RV hemodynamic data. These measures are compared to test how hemodynamically derived RVSWI may underestimate RV function, particularly in the case of tricuspid regurgitation, and whether including regurgitant flow in RVSWI improves predictiveness of RV failure.

In chapter three, RV free wall and septal wall strain is measured using CT. This separates native RV free wall function from the interventricular function of the septal wall. Additionally, the difference between free wall and septal wall strain is analyzed to test whether the RV can compensate for the loss of septal wall function. These strains are then examined in the context of RV preload (end diastolic volume) and afterload (mean pulmonary pressure) to produce three distinct phenotypes of advanced heart failure. These measures are then tested for their ability to improve prediction of RV failure.

CHAPTER 1: CT-derived RV Volumetry Analysis of the Right Ventricle in Heart Failure

1.1 Abstract

Identification of patients who are at a high risk for right ventricular failure (RVF) after left ventricular assist device (LVAD) implantation is of critical importance. Conventional tools for predicting RVF, including 2-dimensional echocardiography, RHC, and clinical parameters, generally have limited sensitivity and specificity. We retrospectively examined the ability of CT ventricular volume measures to identify patients who experienced RVF after LVAD implantation. Between 9/2017 and 7/2021, 90 patients underwent LVAD surgery at our institution. Preoperative CT-derived ventricular volumes were obtained in 19 patients. Patients who underwent CT evaluation had a similar demographics and rate of RVF after LVAD as patients who did not undergo cardiac CT imaging. In the study cohort, 7/19 (36.8%) patients experienced RVF (2 unplanned BiVAD, 5 prolonged inotropic support). CT-derived RV end-diastolic (RVEDVI) and end-systolic volume indices (RVESVI) were the strongest predictors of RVF compared to demographic, echocardiographic, and right heart catheterization data with areas under the receiver operating curve of 0.786 and 0.762 respectively. CT volumetric assessment of RV size can be performed in patients evaluated for LVAD treatment. RV measures of size provide a promising means of pre-LVAD assessment for postoperative RV failure.

1.2 Introduction

Left ventricular assist devices (LVADs) can serve as both a destination therapy for heart failure patients ineligible for transplant or as a bridge-to-transplantation[44]. However, right ventricular failure (RVF) after LVAD implantation is a major cause of morbidity and mortality

[45]. As such, prior research has tried to identify pre-operative parameters to create RVF risk scores, such as the Michigan risk score[46], Fitzpatrick risk score[47], and EUROMACS risk score[29].

Meta-analysis has identified poor right ventricular (RV) performance metrics as predictive of postoperative RVF[27]. Currently, the strongest validated predictor of post-LVAD RV failure is preoperative, qualitative assessment of RV size and function with 2D echocardiography[27, 48]. However, 2D evaluation and qualitative scoring is thought to limit accuracy [49]. Quantitative, 3D evaluation with echocardiography has identified RV dilation and depressed RV ejection fraction (RVEF) as predictors of RVF [50–52], but it can be less accurate when evaluating large RV volumes [53] and require specialized data acquisition and processing (which limits clinical availability).

Predictive parameters also include measurements from right heart catheterization (RHC) such as right atrial pressure (RAP) and right ventricular stroke work index (RVSWI), the product of mean pulmonary arterial pressure and stroke volume. Pulmonary artery pulsatility index (PAPI), the ratio of pulmonary pulse pressure to RAP, has been able to identify high risk patients[54–56] but was not evaluated in the meta-analysis by Bellavia et al[27].

Alternatively, ECG-gated CT angiography (cine CT) – where multiple CT images are acquired across the full cardiac cycle – can be used to perform volumetric RV assessment and values have been validated against cardiac magnetic resonance imaging[42]. Patients evaluated for LVAD implantation routinely undergo non-contrast, chest CT evaluations as part of their work-up to optimize LVAD placement[57]. However, to-date, the utility of volumetric assessment from ECG-gated 3D cine CT has not been reported in patients undergoing LVAD implantation. In this study, we tested the hypothesis that CT-derived preoperative measures of

RV enlargement and decreased systolic function predict RVF after LVAD implantation. As a secondary aim, we compared performance of cine CT-derived metrics of RV function to clinical parameters previously found to be predictors of RVF – namely older age, female gender, elevated INR, low RV stroke work index (RVSWI), elevated RAP, elevated PAPI, and moderate-to-severe right ventricular dysfunction and enlargement on qualitative echocardiographic assessment.[28].

1.3 Materials and Methods

1.3.1 Study Population

Under IRB approved waiver of informed consent, 90 consecutive patients who underwent LVAD implantation between September 2017 and July 2021 were reviewed as part of our retrospective study. The inclusion criteria for enrollment were LVAD implantation at our institution, lack of congenital heart disease, and the availability of clinically-acquired preoperative RHC and echocardiographic assessments as a workup for LVAD or transplant. 65 of the 90 LVAD patients met the inclusion criteria.

In 2017, a cineCT protocol (described below) was implemented for patients undergoing LVAD evaluation. CT evaluation of RV function, including evaluation of RV volumes, 1) was performed in patients who underwent imaging at our institution and 2) was targeted to patients with GFR > 40 mL/min given the concern for kidney injury. Of the 65 patients, 22 had cine CT imaging prior to subsequent LVAD implantation. 21/22 had GFRs > 40 mL/min. 3 patients were excluded due to clinically-documented worsening of ventricular function and ventricular enlargement between the time of cine CT imaging and LVAD implantation surgery. This resulted in a study cohort of n=19 with pre-LVAD CT imaging and comparison cohort of n=43

without CT imaging. Demographic, blood biomarkers, RHC, and echocardiographic parameters for both groups are shown in **Table 1.1**.

1.3.2 Blood Biomarkers and RHC Assessments

Blood biomarkers and RHC measurements before LVAD surgery were obtained as part of standard preoperative care. Pulmonary vascular resistance (Woods units) was calculated as mean arterial pressure - pulmonary capillary wedge pressure over cardiac output. RV stroke work index (RVSWI, g m^{-3} $beat^{-1}$) was calculated as (mean pulmonary arterial pressure - right atrial pressure) x stroke volume index.

1.3.3 Echocardiography

2-dimensional echocardiography was performed before LVAD implantation as part of standard preoperative care. The right ventricle was evaluated qualitatively as having either normal or reduced function. Right ventricular size was qualitatively evaluated as either normal or mild, moderately, or severely enlarged. Tricuspid valve regurgitation was evaluated on a scale of none, mild, moderate, or severe regurgitation. Tricuspid annular plane systolic excursion (TAPSE) was measured on a four chamber view and reported in millimeters.

1.3.4 Computed Tomography

Cine CT imaging was performed on a 256-slice Revolution CT scanner (GE Healthcare, Chicago, IL). All patients were examined in the supine position. After a scout image was taken, a single axial slice was selected to monitor contrast arrival. 80 to 120 ml of contrast agent (Omnipaque; GE Healthcare, Chicago, IL) was injected, followed by a saline flush, all at 4 mL/s.

The scans were performed during a single breath-hold, using retrospective ECG gating. The kVp (80 to 120 kV) and x-ray tube current (400 to 600 mA) were determined based on a clinical imaging protocol. Axial images were reconstructed at 10% intervals across the cardiac cycle (0 to 90% of the R-R). Volumetric evaluation was performed by cardiothoracic-trained radiologists and end-diastolic volumes, end-systolic volumes, stroke volumes, and ejection fractions were reported for the right and left ventricles.

1.3.5 Right Ventricular Failure after LVAD Implantation

The primary outcome was severe RVF after LVAD implantation as defined by INTERMACS criteria [58]: prolonged (≥14 days) need for inotropes in the setting of elevated filling pressures (RAP > 15 mmHg) or the unplanned placement of a right ventricular assist device (RVAD) within a month following LVAD surgery.

1.3.6 Associations with RV Failure

Prediction of post-LVAD RVF from pre-implantation CT-derived volumetric parameters was evaluated using area under the receiver-operating-characteristic curves (AUROC). Confidence intervals were calculated using the approach outlined by Hanley and McNeil[59] for continuous variables. Previously reported predictors of RVF (older age, female gender, elevated INR, low RVSWI, elevated CVP, elevated PAPI, and moderate-to-severe right ventricular dysfunction on echocardiography) were compared to CT-derived measures of RV size and function. Significant predictors of RVF were subsequently analyzed using ROC curves to identify an optimal cutoff point and we report sensitivity and specificity.

1.3.7 Statistical Analysis

Continuous variables are represented as mean ± standard deviation (SD) and were compared with the use of Student unpaired t-test. Variables that were not normally distributed are represented as median with interquartile range values (Q1 to Q3), and differences were analyzed with the Wilcoxon rank sum test. Normality was evaluated using the Shapiro-Wilk test. Categorical variables are presented as percentages and were compared using the Fisher exact test. Univariate logistic regression was used to identify parameters that were predictive of a binary outcome.

1.4 Results

1.4.1 Study Population

Table 1.1 describes the demographics, blood biomarkers, RHC, and echocardiography measures of our cohort. There were no statistically significant differences between patients who underwent cine CT and those who did not in terms of baseline characteristics (gender, age, body mass index, or prevalence of ischemic cardiomyopathy). Further, there was no difference in rate of right ventricular failure after LVAD implantation (36.8 vs 30.2%, p=0.827).

Patients who underwent cine CT had lower median BUN (21 vs 35 mg/dL, $p = 0.009$), lower creatinine (1.16 vs 1.60 mg/dL, $p = 0.001$), higher GFR (76 vs 46, $p < 0.001$), lower bilirubin (0.56 vs 1.05 mg/dL, $p = 0.011$), and higher hematocrit (36% vs 33%, $p = 0.013$) than patients who did not undergo cine CT imaging. There was no significant difference in AST, Albumin, INR, and white blood cell count between populations.

RAP/PCWP ratio was lower (median: 0.39 vs 0.50, p=0.042) in patients who underwent cine CT. Otherwise, there were no significant differences in catheterization-derived parameters including heart rate (HR), right atrial pressure (RAP), pulmonary capillary wedge pressure (PCWP), systolic (PAs), diastolic (PAd), or mean pulmonary pressure (MPAP), pulmonary vascular resistance (PVR), cardiac index (CI) or right ventricular stroke work (RVSWI).

There were no significant differences in qualitative evaluation of RV size, dysfunction, tricuspid regurgitation (TR), or TAPSE on echocardiography. Cine CT-derived measures of RV size and function were successfully obtained in all cases that underwent scanning.

Table 1.1: Comparison of patients with and without CT scan. Patients scanned with ECG-gated cine CT were had expectedly better BUN, creatinine, GFR, bilirubin, and hematocrit values given enrollment criteria. Bold indicates significant different ($p < 0.05$).

	ECG-gated cine CT (n=20)	**Without cine CT (n=43)**	***p*-value**
Demographics			
Gender Female (%)	0	14	0.195
Age (years)	59 (45-71)	60 (46-74)	0.823
BMI (kg/m^2)	27.0 (23.7-30.8)	27.2 (22.7-32.8)	0.865
Ischemic HF (%)	40	46	0.834
Blood Biomarkers			
BUN (mg/dL)	22 (16-27)	35 (22.3-49)	**0.008**
Creatinine (mg/dL)	1.14 (0.83-1.48)	1.60 (1.19-2.19)	**0.001**
GFR (mL/min)	79 (56-90)	46 (31-65)	**0.001**
Bilirubin (mg/dL)	0.58 (0.50-1.06)	1.05 (0.60-1.76)	**0.028**
AST (units/L)	24 (18-31)	28 (20-40)	0.154
Albumin (g/dL)	4.0 (3.6-4.2)	3.8 (3.4-4.2)	0.110

Table 1.1: Comparison of patients with and without CT scan. Patients scanned with ECG-gated cine CT were had expectedly better BUN, creatinine, GFR, bilirubin, and hematocrit values given enrollment criteria. Bold indicates significant different ($p < 0.05$). (cont)

	ECG-gated cine CT (n=20)	**Without cine CT (n=43)**	***p*-value**
INR	1.4 (1.3-2.0)	1.4 (1.2-1.8)	0.721
WBC (10^9 cells/L)	7.2 (5.1-9.4)	8.4 (5.9-10.9)	0.074
Hematocrit (%)	37 (5)	33 (6)	**0.012**
Catheterization			
HR (bpm)	88 (13)	90 (19)	0.780
RAP (mmHg)	8 (5 - 11)	10 (7-15)	0.135
PCWP (mmHg)	23 (10)	23 (9)	0.824
RAP/PCWP	0.38 (0.28-0.48)	0.5 (0.36-0.59)	**0.024**
PAs (mmHg)	46 (16)	50 (14)	0.357
PAd (mmHg)	25 (10)	26 (9)	0.700
MPAP (mmHg)	33 (12)	35 (11)	0.565
PVR (Woods)	2.0 (1.3-2.9)	2.6 (2.0-4.8)	0.067
CI (L/m^2)	1.97 (1.47-2.48)	1.94 (1.34-2.57)	0.853
RVSWI ($g\ beat^{-1}\ m^{-3}$)	7.1 (3.0)	6.7 (3.3)	0.593
PAPI	3.2 (1.9 – 3.8)	2.5 (1.8 – 3.4)	0.189
Echocardiography			
RV dysfunction (%)	70	86	0.244
RV enlargement (%)	13	19	0.832
Mod-Sev TR (%)	30	44	0.427
TAPSE (mm)	1.5 (1.3-2.1)	1.4 (1.1 - 1.7)	0.651
Outcome			
RVF (%)	35.0	30.2	0.930

1.4.2 LVAD Implantation and Development of RV Failure

In our study cohort, the median time from cine CT scan to LVAD implantation was 32 days (IQR 14 - 64). Of the LVADs implanted, 17 patients received Heartmate III (Abbott, Chicago, IL) devices while 2 received Heartware HVAD (Heartware, Framingham, Massachusetts) devices.

7/19 (36.8%) patients with pre-LVAD cine CT imaging developed postoperative right ventricular failure. 2 of these patients required spontaneous RVAD implantation and 5 required long term (≥14 days) inotropic support.

1.4.3 Association of pre-LVAD Clinical Parameters with RV Failure

In our study cohort with imaging (n=19), there were no significant differences ($p > 0.05$) in previously reported predictors of RVF including age, gender, INR, qualitative scoring of RV enlargement or dysfunction on echocardiography, RAP, RAP/PCWP, RVSWI, or PAPI between patients that experienced postoperative RVF and those that did not (**Table 1.2**). In the overall cohort (n=62), only RAP was significantly different in patients who experience RV failure after LVAD implantation (RVF: 13 ± 7 mmHg vs No RVF: 9 ± 4 mmHg, $p = 0.03$).

1.4.4 Association of pre-LVAD Volumes with RV Failure

Patients with RVF had significantly increased indexed right ventricular volumes measured with CT (RVEDVI: 162 ± 43 mL vs 111 ± 37 mL, $p = 0.014$; RVESVI: 120 ± 38 mL/m^2 vs 79 ± 38 mL/m^2, $p = 0.020$). Indexed RV stroke volume was not significantly different ($p = 0.136$) between patients with and without RVF. The resulting difference in RV ejection fraction (with RVF: 24 ± 11% vs without: 31 ± 11%, $p = 0.090$) did not reach statistical

significance. These findings, along with association of pre-LVAD clinical parameters with RVF, are summarized in **Table 1.2**.

Table 1.2: Association of pre-LVAD parameters with RV Failure after LVAD in patients who underwent pre-LVAD CT. RV EDVI and ESVI were significantly increased in patients with RVF with AUC of 0.78 and 0.75 respectively. Bold indicates significant different ($p < 0.05$).

	No RVF (n=13)	RVF (n=7)	*p*-value	AUC
Demographics				
Age (years)	60 (14)	57 (18)	0.628	0.55
Female Gender (%)	0	0	1	N/A
Blood Biomarker				
INR	1.5 (1.3-2.3)	1.3 (1.3-1.4)	0.200	0.68
2D Echocardiography				
RV Enlargement (Mod-Sev) (%)	42	71	0.203	N/A
RV Dysfunction (%)	69	100	0.256	N/A
Hemodynamics				
RAP (mm Hg)	8 (5-9)	12 (6-22)	0.110	0.72
RAP/PCWP ratio	0.35 (0.27-0.41)	0.40 (0.31-0.64)	0.409	0.65
RVSWI (g $beat^{-1}$ m^{-3})	6.7 (4.7-8.7)	8.1 (3.5-12.3)	0.381	0.55
PAPI	1.8 (1.0-5.1)	3.4 (2.5-3.8)	0.692	0.66
Intraoperative Parameters				
Noted Complication (%)	0	0	1	NA
Bypass Time (min)	68 (60-79)	70 (59-94)	0.634	0.571
Cell Salvage (mL)	385 (225-450)	400 (325-450)	0.463	0.615
Crystalloid Infusion (mL)	626 (250)	464 (137)	0.651	0.703
RV CT Assessment				
RV EDVI (mL/m^2)	112 (37)	162 (43)	**0.007**	0.79
RV ESVI (mL/m^2)	81 (38)	120 (38)	**0.023**	0.76
RV SVI (mL/m^2)	32 (27-37)	39 (32-44)	0.096	0.74
RV EF (%)	30 (11)	24 (11)	0.131	0.63

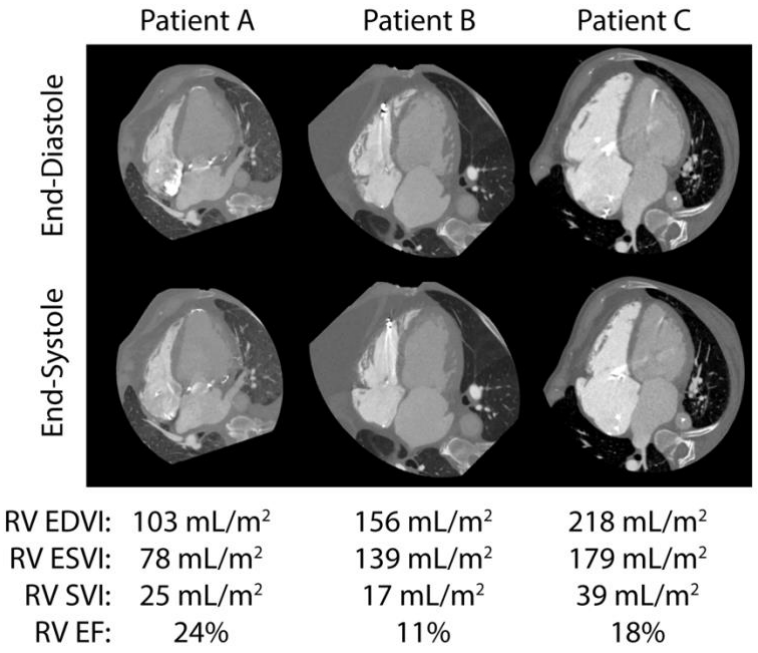

Figure 1.1 Four-chamber images of three patients who underwent CT-based evaluation of RV size and function prior to LVAD implantation. All have mild RV enlargement and reduced RV function on echocardiographic assessment. Patient A did not experience post-operative RVF while patients B and C required prolonged inotropic support.

Univariate logistic regression confirmed RV EDVI (χ^2= 6.196, p = 0.013) and RV ESVI (χ^2= 4.515, p = 0.034) as predictors of RVF.

ROC analysis for CT-derived predictors yielded a higher area-under-the-curve (AUC) for RV EDVI (0.79 ± 0.12) than RV ESVI (0.76 ± 0.13) (**Figure 2**). CT-derived predictors yielded a higher AUC than Age (0.53 ± 0.15), INR (0.67 ± 0.14), RAP (0.71 ± 0.13), RVSWI (0.57 ± 0.15), and PAPI (0.56 ± 0.14).

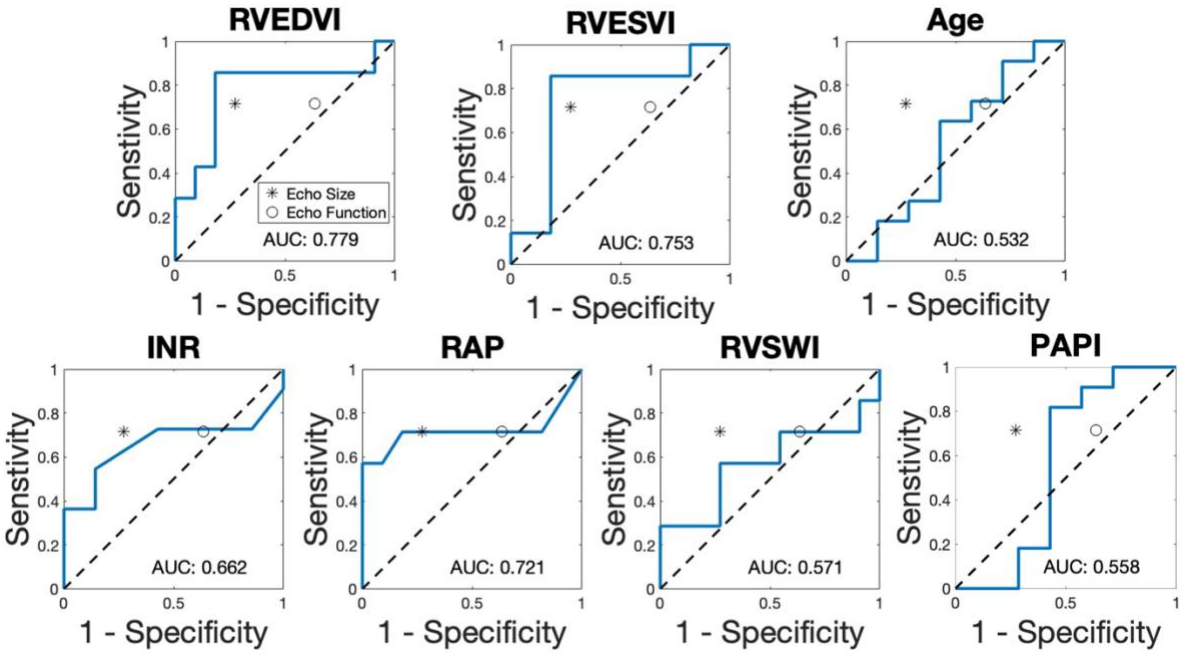

Figure 1.2 ROC curves of RVEDVI, RVESVI, Age, INR, RAP, RVSWI, and PAPI. RV EDVI and RV ESVI each had higher AUC values than the other clinical parameters. Sensitivity and specify of moderate-to-severe enlargement and reduced function on echocardiography are indicated as an asterisk and open circle respectively.

RVEDVI >150mL/m^2 and RVESVI >110 mL/m^2 identified patients who went on to have RVF with 85.7% sensitivity and 83.3% specificity. The optimal cutoff value for age was > 80 years (sensitivity: 90.9%, specificity: 28.6%), INR was < 1.4 (sensitivity: 75.0%, specificity: 57.1%), RAP was > 12 mmHg (sensitivity: 42.8%, specificity:100%), RVSWI was > 382 g m^{-3} $beat^{-1}$ (sensitivity: 28.6%, specificity: 100%), and PAPI was > 1.88 (sensitivity: 83.3%, specificity: 42.8%)

Table 1.3 Sensitivity, Specificity and Cutoff value for RVEDVI and RVESVI in terms of predicting RVF. Of the continuous parameters available for AUC analysis, RV EDVI and ESVI had the highest discriminatory power (AUC of 0.78 and 0.75 respectively).

	Optimal Cutoff	Sensitivity	Specificity	AUC
RV EDVI	150 mL/m^2	85.7	84.6	0.79 ± 0.12
RV ESVI	110 mL/m^2	85.7	76.9	0.76 ± 0.13
Age	80 years	76.9	14.3	0.55 ± 0.15
INR	1.4	85.7	53.9	0.68 ± 0.14
RAP	12 mmHg	57.1	100	0.72 ± 0.13
RVSWI	8 $g\ m^{-3}\ beat^{-1}$	57.1	69.2	0.55 ± 0.14
PAPI	1.88	76.9	57.1	0.66 ± 0.14
Echo Size	>Moderate Enlarged	69.2	71.4	N/A
Echo Function	Depressed	30.7	71.4	N/A

1.5 Discussion

In a retrospective analysis of patients being evaluated for LVAD implantation, we obtained ECG-gated 3D cine CT estimates of RV size and function prior to LVAD implantation. In our cohort, we found preoperative CT-derived right ventricular volumes were significantly larger in patients who had postoperative RVF than those who did not. Additionally, cine CT-derived RV EDVI and ESVI were better predictors than conventional RHC, blood biomarker, or demographic measures. To our knowledge, this is the first use of cine CT to assess RV function prior to LVAD implantation. Our findings add to the body of research that examines preoperative RV volumes and affirms that preoperative CT-derived ventricular volumetric enlargement predicts postoperative RVF.

Our results largely agree with findings from prior studies using 3D echocardiographic assessment of RV volumes and function for patients undergoing LVAD implantation. Specifically, Kiernan et al [50] measured preoperative RV volumes in a similarly sized (n=26) cohort using 3D echocardiography and found RV EDVI and RV ESVI to be significantly larger in patients who went on to have RVF and that 2D echocardiography measures were not different. They also found RVF patients had reduced RVEF, though this relationship did not hold after accounting for RVSWI in multivariate analysis.

Additionally, Otten et al[52] examined preoperative RV volumes using 3D echocardiography and found RV enlargement, similar to those in Kiernan et al, led to higher 60-day mortality. However, patients with severe enlargement RV EDVI (>82 ml/m^2) appeared to be protected effect from 90-day mortality. Magunia et al[51] examined 3D echocardiography metrics in 26 patients and, unlike other studies, did not find a significant difference in volumes for patients with and without RVF. However, they did observe significant differences in function (reduced RVF and reduced RV free wall strain).

The RV volumetric sizes we report in our cohort are larger than those reported by Kiernan et al and by Magunia et al. This could be due to echocardiography limitations in measuring severe RV enlargement or differences in patient population. Only one patient (5%) in our cohort presented as INTERMACS Profile 1 during evaluation, while Kiernan et al had 50% INTERMACS Profile 1 patients and Magunia et al. had 12% INTERMACS Profile 1 patients.

In addition to echocardiography and CT, MRI can be used to obtain RV volume metrics. However, use of MRI in this population is limited by the severity of their heart failure and high prevalence of devices such as balloon pumps and ICDs. For example, 83% (n=15) of our cohort who underwent CT imaging had implanted ICDs and 16% (n=3) had implanted balloon pumps.

MRI is particularly limited by the extended time duration and breath hold requirements in the heart failure population.

RVF is believed to arise from a host of factors, which motivates multifactorial evaluation. For example, most risk scores combine RHC, demographics, and direct echocardiographic assessment of RV function[46, 47, 60]. Our findings suggest that cine CT could be used to augment this type of multifactorial assessment by providing robust quantitative evaluation of RV function. Given that patients typically undergo non-contrast CT as part of the surgical evaluation, cine CT is well position to assess RV size and function robustly and routinely. This may aid when considering whether the patient may benefit from a biventricular assist device (BIVAD) in place of an LVAD.

This study has several limitations. First, this is a retrospective, single-center cohort analysis. As a result, we did not prospectively evaluate the prognostic ability of the proposed RV EDVI or ESVI cutoff values. Additionally, the small sample size limits the use of multivariate analysis. Further, timing between CT scanning and LVAD implantation was variable within the cohort (IQR 14 - 64 days); however, patients with significant changes in cardiovascular status between imaging and implantation were excluded via record review. Cine CT requires the use of iodinated contrast and our imaging protocol targeted patients with GFR > 40mL/min. As a result, patients with GFR < 40mL/min were overrepresented in the comparison cohort that did not receive CT scanning due to kidney injury concerns. As expected, this led our study cohort with CT to have better renal function than patients who did not undergo contrast-enhanced CT, as shown in **Table 1.1**. While our scanned population had lower RAP/PCWP, a parameter that may portend risk of RVF, rates of RVF were similar between the scanned and non-scanned groups. The relationship between RV volumes and RVF may reflect a relationship between loading

conditions and RVF, and the association of RV volumes with RVF should not be regarded as causal. Further prospective studies into the relationship between RV volumes, including volumetric changes during clinical care, and RVF are needed to validate these findings. These studies should also consider perioperative findings such as surgical times which may also be associated with RVF. Future work aims to investigate the utility and safety of cine CT scanning in patients with lower renal function so that CT-derived volumetric evaluation can be expanded to the broader population of patients undergoing LVAD evaluation.

1.6 Conclusion

ECG-gated contrast-enhanced CT imaging can be used to obtain volumetric, quantitative measures of RV size and function in heart failure patients being evaluated for LVAD implantation. CT-derived RV enlargement was associated with a higher risk of RVF. Given that patients typically undergo non-contrast CT as part of the surgical evaluation, use of cine CT could augment clinical evaluations and further establish routine assessment of RV size and function.

1.7 Acknowledgements

Chapter 1, in part, is a reprint of the material as it appears as “Preoperative Computed tomography Assessment of Risk of Right Ventricular Failure” in the journal *American Society for Artifical Internal Organs*, 2022 by Anderson Scott, Seth Kligerman, Diana Hernandez Hernandez, Kim Paul, Hao Tran, Victor Pretorius, Eric Adler, and Francisco Contijoch. The dissertation author was the primary investigator and author of this paper.

CHAPTER 2: Pressure Volume Loop Analysis of the Right Ventricle with Computed Tomography in Heart Failure

2.1 Abstract

Right ventricular (RV) function is an important marker of mortality for patients with chronic left-sided heart failure. RV function is particularly important for patients receiving a left ventricular assist device as it is a strong predictor of post-operative RV failure. RV stroke work index (RVSWI), defined as the area enclosed by a pressure volume (PV) loop, is a prognostic metric of RV function. However, clinical RVSWI approximates this area as the product of thermodilution-derived stroke volume and the pulmonary pressure gradient. This ignores the energetic contribution of regurgitant flow and does not allow for advanced energetic measures, such as pressure volume area and efficiency. While clinical RVSWI is important for assessing patient wellness, capturing forward flow may underestimate underlying RV function. We developed an approach to create single-beat PV loops by combining data from cine computed tomography (CT) and right heart catheterization in 44 heart failure patients. We tested the approximations by clinical RVSWI and found it to underestimate PV loop RVSWI, primarily due to regurgitant flow in tricuspid regurgitation. The ability of RVSWI to predict post-operative RV failure improved in a statistically significant fashion when the single-beat approach was used. Further, RV pressure volume area and efficiency measures were obtained and show broad agreement with other functional measures. Future work is needed to investigate the utility of these PV metrics in a clinical setting.

2.2 Introduction

Right ventricular (RV) performance is increasingly recognized as a key metric in the evaluation of patients with left-sided cardiac dysfunction[61] as measures of RV systolic function such as RV ejection fraction (RVEF)[62, 63] and RV longitudinal shortening[39, 64] have been shown to predict survival in heart failure patients. Pulmonary arterial (PA) pressure measurements have also been shown to improve evaluation with RV volumes alone; Ghio et al[65] found the ability of RVEF to predict freedom from urgent transplantation strengthened in the context of elevated pulmonary pressure.

RV stroke work index (RVSWI) measures the energetic work performed by the ventricle by integrating volume and pressure values during the cardiac cycle. RVSWI has been shown to predict right ventricular dysfunction after implantation of left ventricular assist devices (LVAD), particularly in the case of elevated central venous pressure[47, 66]. However, due to poor specificity, RVSWI has had limited prognostic value in preoperative LVAD assessment in follow-up studies[27]. We hypothesize that the limited specificity is due to how RVSWI is measured. Specifically, the gold standard measurement of RVSWI is the area encapsulated in a pressure volume (PV) loop from RV conductance catheterization[67] normalized by the body surface area (BSA). Clinically, this PV loop area is approximated as a rectangle with forward stroke volume (measured via thermodilution) as the width and mean pulmonary pressure difference (difference between mean pulmonary and right atrial pressure) as the height. While this approximation enables estimation from a right heart catheterization (RHC), it introduces potential pitfalls and precludes measurement of other PV loop-based metrics.

Recently, ECG-gated computed tomography (CT) evaluation of RV function has been shown to predict RV failure after LVAD implantation in heart failure [68]. However, whether this evaluation can be improved by leveraging pressure information is unknown. In this study, we combine CT-derived RV volumetry with RV pressure recordings from contemporaneous RHC to generate single-beat RV PV loops from which we measure RVSWI and other advanced measures. We use this framework to evaluate the assumptions used in clinical RVSWI measurements in heart failure patients undergoing evaluation for advanced therapies. We hypothesize that clinical RVSWI will underestimate RV performance (relative to CT-based estimation) in patients with regurgitant stroke volume.

While forward stroke volume and stroke work index may be strongly associated with patient wellness, regurgitant stroke volume and its corresponding stroke work may be an important factor of RV function, which is the most significant predictor of RVF in meta-analysis[27]. Therefore, we expect that incorporating the contribution of regurgitant flow may improve the prognostic ability of RVSWI in predicting RV failure after LVAD implantation, particularly in patients with tricuspid regurgitation (TR). Further, by creating single-beat PV loops, we expect our approach will enable us to further characterize RV function via additional, energetics-based metrics - PV area (PVA)[69] and RV efficiency[70].

2.3 Methods

2.3.1 Population

With IRB waiver of informed consent, records of non-congenital heart failure patients who underwent cardiac cineCT scanning between September 2017 and September 2021 were retrospectively reviewed to identify patients undergoing work-up for advanced therapies.

Patients were included if they received a right heart catheterization within two weeks of the cineCT scan. Exclusion criteria included incomplete or missing pressure waveform recordings, poor contrast-to-noise ratio in the CT images, defined as the ratio of the absolute difference between blood pool and myocardial pixel intensity to the standard deviation of the image noise as less than 5, or documented changes in appearance or care that would affect either pressure or volume readings between the two studies, such as changes in cardiac silhouette and documented changes in diuretics or urinary output. RV failure in patients who received a left ventricular assist device (LVAD) was determined using the updated consensus of adverse events of mechanical circulatory support[71].

2.3.2 CT-derived parameters

CineCT imaging was performed on a 256-slice Revolution CT scanner (GE Healthcare, Chicago, IL). All patients were examined in the supine position. After a scout image was taken, a single axial slice was selected to monitor contrast arrival. 80 to 120 ml of contrast agent (Omnipaque; GE Healthcare, Chicago, IL) was injected, followed by a saline flush, all at 4 mL/s. The scans were performed during a single breath-hold, using retrospective ECG gating. The kVp (80 to 120 kV) and x-ray tube current (400 to 600 mA) were determined based on a clinical imaging protocol. Axial images were reconstructed at 10% intervals across the cardiac cycle (0 to 90% of the R-R). Effective dose length product was estimated to be between 200 and 500 mGy*cm. Ventricular volumes such as right ventricular end-diastolic volume (RVEDV), end-systolic volume (RVESV), and stroke volume (SV_{CT}), as well as ejection fraction (RVEF) were obtained from a volume curve, V(t), spanning one cardiac cycle.

2.3.3 RV Blood Pool Volume Segmentation

RV blood pool volume was derived using a 2D U-Net based deep learning framework that has been previously shown to accurately segment blood chambers in cardiac CT angiograms[72]. This 2D U-Net functions by taking z-axis slices of the multidimensional array of cardiac scans and predicting on the 2D image. The model predicts a 2D array of 0's and 1's to label the estimated location of a pixel within the right ventricle. After all images have passed through the predictive model, the images are then collated to reform 3D volumes. This model was trained on two manually segmented time frames for each patient in this cohort, end systole and end diastole. This model was validated on 20 patients for whom all CT scans of the heart had been manually segmented during the cardiac cycle. Each patient typically had 10 scans during the cardiac cycle. Each scan had approximately 500 2D images along the z-axis per scan. This resulted in a training set of 50,000 images and a validation set of 8,000 images. The 2D U-Net performed with a DICE coefficient of 0.90 in the validation set. Segmentations were created using the U-Net for all patient volume curves. Segmentations generated by the deep learning approach were visually inspected to verify that segmented blood volumes were anatomically correct and temporally consistent.

2.3.4 RHC waveform analysis

RHC records within 2 weeks of the cineCT scan were reviewed to extract thermodilution-based estimate of cardiac output (CO_{RHC}), heart rate (HR), mean pulmonary artery pressure (mPAP), right atrial pressure (RAP), end-systolic and end-diastolic right ventricular pressures (RVSP and RVDP). From these values, we derived right ventricular pulse pressure (RVPP) as the difference between RVSP and RVDP, stroke volume (SV_{RHC}) as the ratio of thermodilution

based cardiac output (CO_{RHC}) to HR, and stroke volume index (SVI_{RHC}) as the SV_{RHC} indexed by body surface area (BSA). As described earlier, SV_{RHC} only captures forward flow through the pulmonary artery. A RHC-based estimate of RVSWI ($RVSWI_{RHC}$) was calculated as the product of SVI_{RHC} and the difference between mPAP and RAP. For PV loop analysis, the RV pressure waveforms obtained during RHC were digitized using a plot digitizing software[73].

2.3.5 Pressure-Volume Loop Estimation

To synchronize RV pressure and volume waveforms and generate Pressure Volume (PV) loops, both signals were resampled to a standard number of points (n=60) using the percentage of cardiac cycle (%RR) as a shared reference. The %RR was determined using ECG signals already synchronized with both the RHC and CT studies. Heart rates were compared to account for possible differences in cardiac function as heart rate increases or decreases. PV loop-based estimation of RVSWI was obtained by integrating the P(t) vs V(t) signal and normalizing by patient BSA. RVSWI calculated using CT PV loops is denoted $RVSWI_{CT}$.

2.3.6 Comparison of clinical RVSWI with single beat CT-RHC synthesis

We compared the catheter-based estimate of pressure difference (mPAP-RAP) to the right ventricular pulse pressure (RVPP) to evaluate the assumption that the right ventricular pulse pressure is the same as the pulmonary and right atrial pressure difference. We also compared thermodilution-derived SV_{RHC} to CT-derived SV_{CT} to evaluate the assumption that thermodilution derived stroke volume captures the blood volume ejected by the RV. Finally, the resulting RVSWI estimates - clinical $RVSWI_{RHC}$ and $RVSWI_{CT}$ – were compared. Differences between SV_{RHC} and SV_{CT} as well as $RVSWI_{RHC}$ and $RVSWI_{CT}$ were evaluated as a function of

tricuspid regurgitation (none-mild vs moderate-severe) as assessed by the most recent clinical echocardiography study.

To evaluate the impact of assuming the PV loop is rectangular in shape, we created a hybrid RVSWI estimate ($RVSWI_{COMB}$) defined as the product of SVI_{CT} and RV pulse pressure. This metric still assumes a rectangular loop shape but corrects for discrepancies introduced by the use SVI_{RHC} and pulmonary pressure. $RVSWI_{COMB}$ was compared to $RVSWI_{CT}$. $RVSWI_{COMB}$ does not require full volumetric or hemodynamic waveforms so can be more easily obtained. Therefore, its ability to predict right ventricle failure in patients who went on to receive an LVAD was compared directly against $RVSWI_{RHC}$ and tricuspid regurgitation.

2.3.7 Advanced Energetic Evaluation: RV Pressure Volume Area and Efficiency

Pressure volume area (PVA) is defined as the sum of the two non-overlapping area of the PV loop diagram: $RVSW_{CT}$ and the ventricular potential energy. Potential energy is the area enclosed by the end-systolic and end-diastolic pressure volume relationship curves (ESPVR and EDPVR, respectively), which can be approximated as the triangular area between the origin, the end-systolic point, and the end-diastolic point[74]. The end-systolic and end-diastolic points were defined as the points with maximum and minimum instantaneous elastance respectively. RV Efficiency is defined as the ratio of stroke work to total PVA. To analyze broad agreement between advanced energetic evaluations and established measures of RV function, RV PVA and efficiency were compared to RV ejection fraction. To evaluate the impact of estimating ESPVR and EDPVR as straight lines which intersect at the origin (i.e., $V_0=0$), we compared PVA and RV efficiency measures to values obtained when V_0 was estimated using two single-beat

approaches – a pressure-based estimation which calculates a theoretical maximum ventricular pressure[75] and a nonlinear modeling approach[76].

2.3.8 Statistical Analysis

Continuous values are reported as mean and standard deviation if normally distributed and as the median and first and third quartile if non-normally distributed. Binary variables are reported as proportions. Correlations between measures are measured using the Pearson's correlation coefficient for continuous variables. Student's t-test was used to test whether the correlation coefficient was significantly different than 0. Difference in stroke volume and difference in stroke work index between different grades of tricuspid regurgitation were compared using an unpaired t-test. The correlations between continuous variables were also analyzed using linear regression modeling. The relationships between the variables were considered strong for absolute correlation value above 0.7, moderate for absolute values above 0.5, mild for values above 0.3, and weak for all lower values. Comparison of predictive potential was done using area under the curve (AUC) of receiver operating characteristic (ROC) curves. AUCs are reported with a 95% confidence interval. A p-value of less than 0.05 was considered significant. All statistical analyses were performed in Matlab R2018b (The Math Works, Inc, Natick, MA).

2.4 Results

2.4.1 Patient Population

54 patients had RHC and CT scanning performed contemporaneously (within 2 weeks) as part of work-up for advanced therapies. 5 patients were excluded due to insufficient RV pressure

waveforms. 5 patients had insufficient contrast-to-noise ratio on cineCT imaging. None of the 44 patients experienced significant change in cardiac silhouette or urinary output in the time between cineCT and RHC (**Figure 1**). The median time between CT and RHC was 2 (interquartile range: 0 - 4) days. Heart rates were not significantly different between the CT and RHC study (CT HR: 84 ± 12 bpm vs RHC HR: 85±18 bpm, $p > 0.05$). The difference between CT and RHC heart rate was -1 ± 10 bpm. Demographics of the 44 patients, our study population, are described in **Table 2.1**. Of the patients, 14 went on to receive an LVAD with RHC and CT scans within 2 weeks and for whom $RVSWI_{COMB}$ could be measured. Of the 14, 6 (46%) went on to have post operative right ventricular failure.

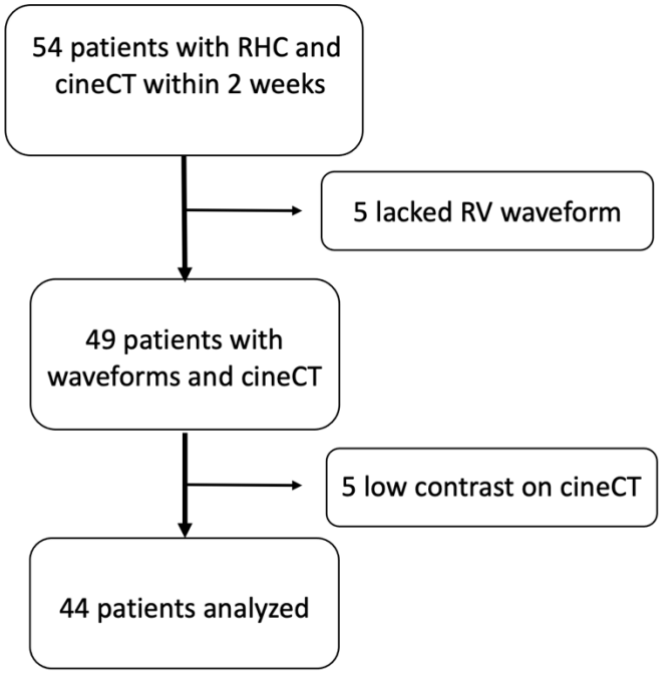

Figure 2.1 Flowchart of patients evaluated for PV analysis. 44 patients were evaluated after removal of patients who had low RV contrast on imaging (n=5) and patients who RHC studies did not have RV pressure waveforms available for analysis (n=5).

Table 2.1 Patient Parameters of the 44 Patient Subcohort

Parameter	**Mean/Median**	**SD/IQR (25%-75%)**
Demographic		
Age (years)	58	50-68
Female (%)	21	-
BMI (kg/m2)	27.1	22.9-29.5
Ischemic HF (%)	14	-
RHC to CT time (Days)	2	0-4
RHC		
CO (L/min)	3.7	1.2
HR (bpm)	85	18
MPAP (mmHg)	31	11
RAP (mmHg)	10	5
PCWP (mmHg)	22	9
PVR (mmHg*min / L)	2.1	1.4-3.6
Echocardiography		
LV Enlargement (%)	38.6	-
LV Dysfunction (%)	90.9	-
RV Enlargement (%)	11.4	-
RV Dysfunction (%)	54.5	-
Mod-Sev TR (%)	29.5	-
CT		
LVEDVI (mL/m^2)	142	120-199
LVESVI (mL/m^2)	110	82-188
LVEF (%)	20	5
RVEDVI (mL/m^2)	123	38
RVESVI (mL/m^2)	86	36
RVEF (%)	32	11

2.4.2 Accuracy of pressure approximation

Mean pulmonary arterial pressure was highly correlated ($\rho = 0.81, p < 0.001$) with RV pulse pressure. However, RV pulse pressure was greater, on average, by 21 mmHg. The standard deviation of the difference was 7 mmHg (**Figure 2B**).

2.4.3 Accuracy of stroke volume approximation and the impact of loop shape

The correlation between SV_{RHC} and SV_{CT} was not statistically significant ($\rho = 0.14, p = 0.35$). Thermodilution-derived SV_{RHC} underestimated SV_{CT} by 30 mL with standard deviation of 29 mL (**Figure 2C**). Clinical $RVSWI_{RHC}$ was mildly correlated with PV loop-derived $RVSWI_{CT}$ ($\rho = 0.36, p = 0.017$) (**Figure 2D**). $RVSWI_{COMB}$ was strongly correlated with PV loop-derived $RVSWI_{CT}$ ($\rho = 0.78, p < 0.001, \text{RVSWI}_{COMB} = 1.2\ \text{RVSWI}_{CT} + 3.5, R^2 = 0.10$).

2.4.4 Impact of tricuspid regurgitation on stroke volume and stroke work

Patients with moderate-to-severe tricuspid regurgitation (TR) had a significantly higher discrepancy in stroke volume between CT and RHC compared to patients with no-to-mild tricuspid regurgitation (median: 40 mL vs 23 mL difference, $p = 0.003$). Patients with moderate- to-severe TR also had a larger discrepancy between $RVSWI_{RHC}$ and $RVSWI_{CT}$ than patients with less TR (median: 2 and 6 gm/beat/m^2, $p = 0.003$) (**Figure 2E**).

Patients with mild or no tricuspid regurgitation (n=30, 68%) had a significant and moderate correlation between $RVSWI_{RHC}$ and PV-derived $RVSWI_{CT}$ ($\rho = 0.56, p = 0.001$). The correlation for patients with moderate or severe tricuspid regurgitation (n=14, 32%) did not achieve statistical significance ($\rho = 0.39, p = 0.086$).

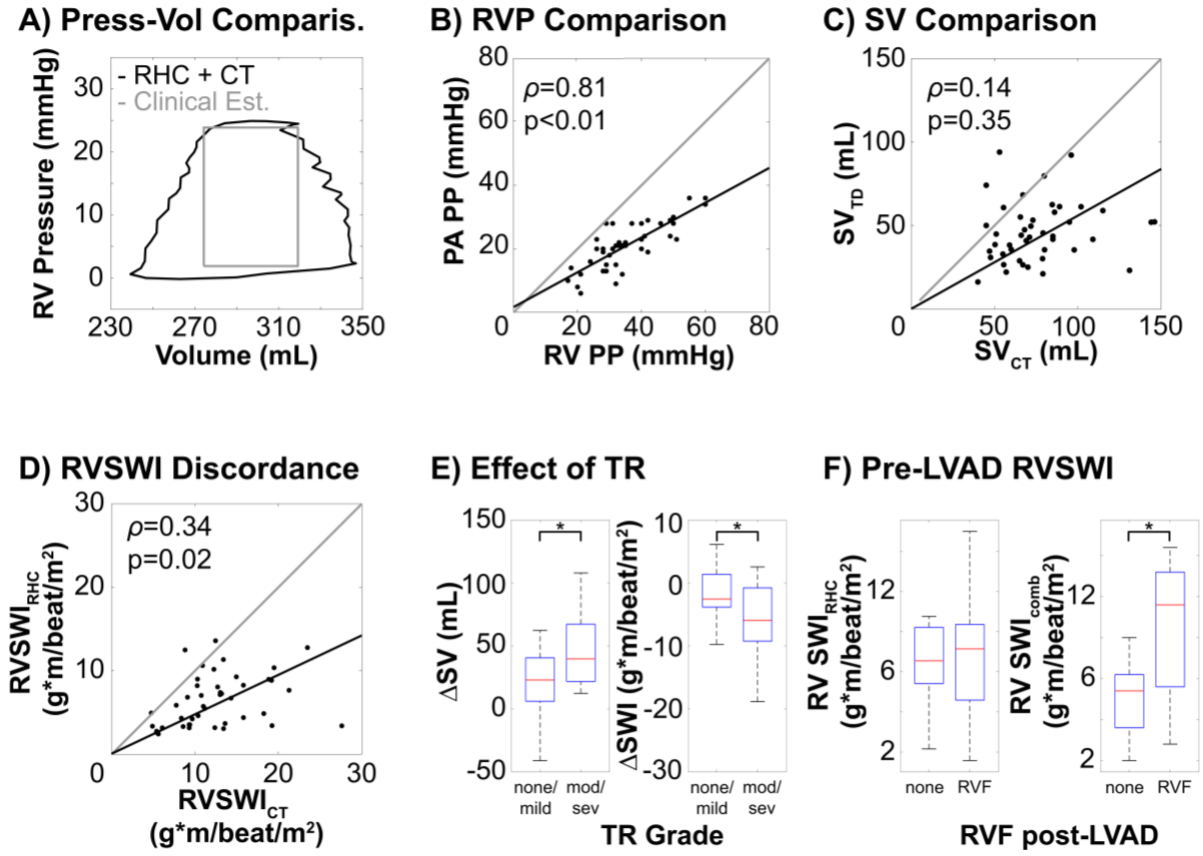

Figure 2.2 Evaluation of Discrepancy between RHC- and PV loop-derived RVSWI. Best fit line (black) and unity line (gray) are shown when relevant. **A)** Comparison between the clinical approximation and single beat approach. **B)** High correlation was observed between mPAP-RAP and RV PP. **C)** RHC- and CT-derived stroke volume was not significantly correlated. **D)** Mild correlation between RVSWI estimates with clinical underestimation. **E)** Differences between SV and SWI were larger in moderate-severe tricuspid regurgitation. **F)** Correcting for underestimation of SV improved separation between patients with and without RVF.

2.4.5 Effect of corrected stroke work index on patient outcomes

Of the 14 patients, 6 (43%) had post-LVAD RVF. Patients with RVF after LVAD implantation did not have significantly different $RVSWI_{RHC}$ than those without (RVF: 6.1 ± 2.9 vs non-RVF: 6.9 ± 3.4, p = 0.33). However, patients with RVF had significantly higher $RVSWI_{COMB}$ than those without RVF (RVF: 21 ± 9 vs non-RVF: 13 ± 5, p = 0.0149) (**Figure 2F**). The AUC for $RVSWI_{COMB}$ (0.81, 95% CI: 0.60-1.0), as a predictor of postoperative failure was significantly higher than $RVSWI_{RHC}$, (0.50, 95% CI: 0.23-0.77).

Of the 14 patients, 4 (29%) had moderate to severe tricuspid regurgitation. Prediction of RVF based on the presence of moderate to severe tricuspid regurgitation had an accuracy of 64% (9/14), specifity of 74%, and sensitivity of 25%.

2.4.6 Advanced energetic measures

Our ability to estimate advanced energetic measures of RV performance is shown in **Figure 3**. Visualizations of these energetic measures are shown in **Figure 3A**. RV efficiency was strongly correlated with RV ejection fraction ($\rho = 0.77, p < 0.001, \mathrm{RVEff} = 1.0\mathrm{RVEF} + 5, \mathrm{R}^2 = 0.59$, **Figure 3B**). PVA had a moderate inverse correlation with RVEF ($\rho = -0.64, p < 0.001, \mathrm{PVA} = -1.3\mathrm{RVEF} + 86, \mathrm{R}^2 = 0.42$, **Figure 3C**).

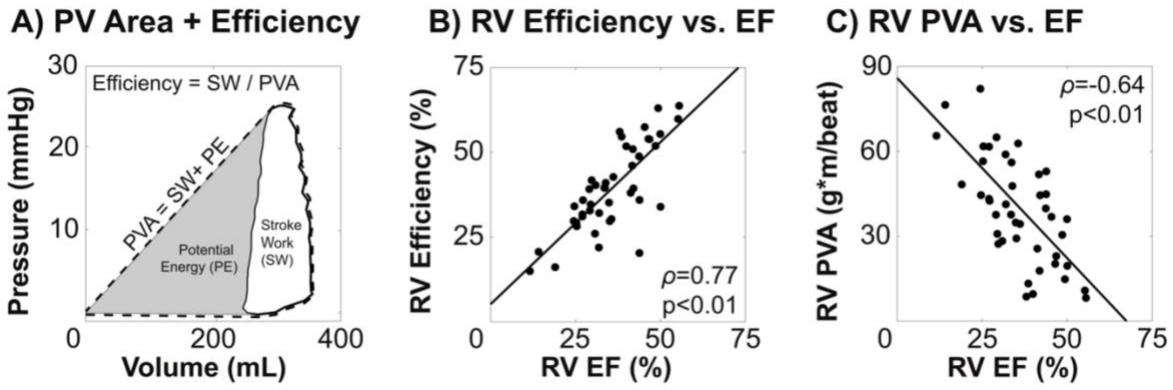

Figure 2.3 Advanced energetic analysis of right ventricular (RV) performance. Best fit line (black) and unity line (gray) are shown when relevant. A) Illustration of pressure volume area (PVA) as the sum of stroke work and potential energy and efficiency as the ratio of stroke work to pressure volume area. B) Strong positive correlation was observed between RV efficiency and ejection fraction (EF) C) Moderate negative correlation was observed between PVA and RV EF.

2.4.7 Impact of V_0 estimate on PVA and RV Efficiency

The method used to estimate V_0 did not have a significant impact on our estimates of PVA and RV efficiency. Estimation of V_0 using the Pmax method succeeded in 38 of the 44 patients. In

these 38 patients, average V_0 was found to be -25 ± 50 mL. This resulted in PVA and efficiency values that underestimated our initial estimate, though were still highly correlated (PVA $\rho = 0.86, p < 0.001$, RV Eff $\rho = 0.91, p < 0.001$). The results from using the nonlinear modeling of V_0 were similar. Modeling succeeded in 36 of the 44 patients. In this group, V_0 was calculated to be 55 ± 26 mL. Again, this led to PVA and efficiency values that were highly correlated to our estimate when V_0=0 (PVA $\rho = 0.92,\ p < 0.001,$ RV Eff $\rho = 0.92,\ p < 0.001$). While this assumption led to a consistent absolute error that would affect proposed cutoff values, it did not affect the relative agreement of PVA or RV efficiency.

2.5 Discussion

This study aimed to demonstrate the ability of hemodynamics and CT imaging to reconstruct PV loops in heart failure patients and augment hemodynamic or volumetry-alone assessment. In patients with heart failure, clinical $RVSWI_{RHC}$ was significantly different than RVSWI obtained using a single beat PV loop approach. While the clinical assumption that RV PP is the same as mPAP leads to small errors ($\rho = 0.81$), thermodilution-derived SV_{RHC} was significantly lower than SV_{CT} obtained with CT. The underestimation of SV by thermodilution was more pronounced in patients with moderate-to-severe tricuspid regurgitation, which affected 30% of the study cohort. PV loop-derived $RVSWI_{CT}$ and clinical $RVSWI_{RHC}$ showed stronger agreement if patients with tricuspid regurgitation were excluded from the analysis (all patients: $\rho = 0.36$ vs patients without TR: $\rho = 0.56$). Correcting for pressure and stroke volume differences (but maintaining a rectangular PV loop shape) led to $RVSWI_{COMB}$ which was similar ($\rho = 0.78$) to the RVSWI estimated by combining RHC and CT data. Lastly, in a subcohort of patients who received an LVAD, correcting RVSWI with CT volumetry showed statistically

significant improvement in the ability of RVSWI to differentiate patients that went on to have RV failure from those who did not using AUC of ROC curves.

Our approach also enabled estimation of advanced energetic measures of RV performance such as pressure volume area (PVA) and ventricular efficiency using clinically obtained studies. We found these measurements complemented volumetric CT measures of RV function (RVEF). Therefore, combining CT with RHC may provide additional prognostic or diagnostic information for patients than RHC alone. While estimates of V_0 were estimated to be nonzero with different approaches, accounting for V_0 had little effect on how patients would be classified based on PVA and efficiency. Further, the Pmax and nonlinear curve fitting methods failed to yield V_0 estimates in 14% and 18% of the patient population, respectively.

While direct Fick is the gold-standard for estimation of cardiac output, estimated Fick and thermodilution are more commonly used in a clinical setting. Studies comparing these two estimates have found significant differences between thermodilution and estimated Fick, with thermodilution being a stronger predictor of mortality [77, 78]. Underestimation of cardiac output in the presence of tricuspid regurgitation is well documented, even using the direct Fick approach [79–81]. In our study, accounting for regurgitant flow ($RVSWI_{COMB}$) strengthened estimation of PV loop derived RVSWI (ρ increased from 0.34 to 0.77). This suggests that clinical estimation of RVSWI could more closely match PV loop estimates if RV stroke volume is measured directly and regurgitant volumes are captured. While $RVSWI_{RHC}$ may be more important for patient wellness, we found that incorporating regurgitant flow into RVSWI had a significantly higher prognostic value (AUC 0.81) for postoperative right ventricular failure greater than either clinical $RVSWI_{RHC}$ (AUC 0.50) or moderate-severe tricuspid regurgitation

alone. This may suggest that including regurgitant flow in RVSWI measures is a better identifier of underlying RV function. This agrees previous data that has found tricuspid regurgitation to be a significant predictor of postoperative RVF on its own. Clinically, this may suggest that CT evaluation of RV volumes, particularly stroke volume, would aid in assessing RV function.

In addition to cineCT, cardiac magnetic resonance (CMR) imaging and 3D echocardiography can be used to obtain RV volume measures. CT has a strong correlation with CMR for RV volumes. However, CMR is difficult to perform in this patient population due to breath hold requirements and high prevalence of implanted cardiac devices. Further, 3D echocardiography is known to underestimate volumes in the setting of RV enlargement [82, 83] and has been shown to have high rates of study exclusion [40, 84] due to imaging difficulties.

PVA (the sum of stroke work and potential energy, Figure 3A) has been shown to linearly correlate with myocardial oxygen consumption in a load independent manner [85, 86]. However, PVA and RV efficiency have seen limited clinical use due to challenges associated with acquiring contemporaneous pressure and volume data in a clinical setting [67]. We demonstrate an approach to combine RHC with CT to generate single-beat PV loops and measure PVA and ventricular efficiency in patients with heart failure. Our results outline a clinically available means for assessing and testing these advanced metrics. Clinically, PVA and efficiency may help differentiate patients who have similar conventional CT metrics of RV function (RVEF and RVEDVI) during RV evaluation by characterizing contractility as in animal models [70]. This complementary function, however, would need to be evaluated in a dedicated study.

There are several limitations to this study. Right heart catheterization (RHC) and CT imaging were not performed simultaneously. However, 27% of patients had CT scans obtained on the same day as RHC evaluation and 66% of patients had CT scans within 3 days of their RHC evaluation. Second, as a retrospective study, conductance catheter measures were not obtained to compare our PV loops to invasive assessment. Third, our study is a single-center retrospective analysis which limited the size of the patient population. Additionally, only 14 patients had a clinical outcome that was evaluated, As a result, the confidence intervals for the AUC of $RVSWI_{COMB}$ (0.60-1.00) and $RVSWI_{RHC}$ (0.23 – 0.77) were broad and these results would require further studies to investigate these findings. Lastly, PV-derived measures were created to test the assumptions of RHC-derived measures and test advanced energetic measures for agreement with functional measures that have been correlated to outcomes. However, the individual clinical benefit of using these PV-derived measures, relative to the current clinical approach, requires additional study.

2.6 Conclusion

CT evaluation may improve evaluation of RV function by combining volumetry with right heart catheterization-derived pressure recordings, particularly in the setting of significant tricuspid regurgitation. This approach enabled evaluation of PV loop-derived RVSWI, which estimated the energetic contribution of regurgitant flow and enabled advanced energetic measures such as pressure volume area and RV efficiency to be obtained clinically in the heart failure population.

2.7 Acknowledgements

Chapter 2, in part, is a reprint of the material as an accepted manuscript as “Pressure Volume Loop Analysis of the Right Ventricle with Computed Tomography in Heart Failure” in the journal *American Society of Artificial Internal Organs*, 2022 by Anderson Scott, Zhennong Chen, Diana Hernandez Hernandez, Seth Kligerman, Paul Kim, Hao Tran, Eric Adler, and Francisco Contijoch. The dissertation author was the primary investigator and author of this paper.

CHAPTER 3: Free Wall and Septal Wall Analysis of the Right Ventricle with Computed Tomography in Heart Failure

3.1 Abstract

Patients in advanced stages of heart failure who receive a left ventricular assist device (LVAD) are at a high risk for right ventricular failure. Presumably this is due, in part, to preoperative RV dysfunction that may be obfuscated by poor LV function. RV free wall strain has been proposed as a predictive metric to evaluate isolated RV function while RV dilation has been shown to be a late prognostic metric of RV failure. CineCT has been used to evaluate both RV strain and RV dilation; however, this analysis has not been done in this patient population. Using cineCT, we quantified RV free wall (FW) and septal wall (SW) strain in patients with end-stage heart failure and in a control group without heart failure. We then tested the relationship between these metrics and loading conditions, namely mean pulmonary pressure and RV end diastolic volume. Finally, for the patients who went on to receive an LVAD, we compared the ability of these CT measures to predict right ventricular failure after implantation.

FW and SW strain were greatly impaired in heart failure patients compared to controls. FW strain was greater than SW strain in heart failure patients, but not controls. This difference between FW and SW strain was not strongly correlated with conventional measures of preload or afterload. FW and SW strain predicted post-implant RV failure with an AUC of 0.69 and 0.67 respectively. The difference between FW and SW strain was the strongest predictor with AUC of 0.82. Using the difference between FW strain and SW strain and RVEDVI, we observed three phenotypes of heart failure patients: patients with preserved EDVI and increased FW strain,

patients with preserved EDVI but no FW compensation, and patients with enlarged EDVI and decreased FW strain.

3.2 Introduction

Right ventricular (RV) function is an important prognostic for survival and other outcomes for patients with heart failure[87, 88]. Non-invasive, clinical imaging-based assessment of RV function, has been limited by the RV's unique shape, heavy trabeculation, and sensitivity to loading conditions[89]. As a result, conventional imaging-derived metrics of dysfunction (i.e., RV dilation and depressed RV ejection fraction on volumetry) do not manifest until late stages of RV dysfunction. Early identification of dysfunction is particularly important to assess risk for patients who go on to have left ventricular assist device (LVAD) who are at an increased risk of RV failure[19].

RV free wall (FW) strain, assessed with speckle tracking echocardiography, has been recently shown to be an early prognostic indicator of underlying RV dysfunction [90–92]. Strong RV FW strain may reflect adaptation of the longitudinal FW shortening in response to depressed septal wall shortening.[93] Conversely, poor FW strain may reflect an inability of native RV FW strain to adapt to the declining septal wall function, and may act as an identifier early dysfunction in heart failure patients.

ECG-gated CT (CineCT) can accurately assess the 3D geometry of the RV and provides accurately volumetry[42]. Further, CineCT has also been used to derive localized measures of strain in the RV[94]. However, the ability of CineCT to measure RV free wall (FW) and septal wall (SW) strain in heart failure patients has not been evaluated. Therefore, in this study, we examine whether FW and SW strain are correlated with loading conditions, analyze the

relationship between RV enlargement, and strain values to identify possible common functional characteristics, and test whether these cineCT strain measures can predict postoperative RV failure.

3.3 Methods

3.3.1 Patient Population

With IRB waiver of informed consent, records of patients who underwent cardiac cineCT between September 2017 and September 2021 were retrospectively reviewed to identify patients with end-stage heart failure who underwent work-up for advanced therapies. RV failure in patients who received a left ventricular assist device (LVAD) was determined using the updated criteria for adverse events in mechanical circulatory support[71]. Patients who received cineCT between 2018 and 2020 before starting anthracycline without any indications of heart failure and normal (>50%) ejection fraction were analyzed as a control non-heart failure population.

3.3.2 CT Imaging

CineCT imaging was performed on a 256-slice Revolution CT scanner (GE Healthcare, Chicago, IL). All patients were examined in the supine position. After a scout image was taken, a single axial slice was selected to monitor contrast arrival. 80 to 120 ml of contrast agent (Omnipaque; GE Healthcare, Chicago, IL) was injected, followed by a saline flush, all at 4 mL/s. The scans were performed during a single breath-hold, using retrospective ECG gating. The kVp (80 to 120 kV) and x-ray tube current (400 to 600 mA) were determined based on a clinical imaging protocol. Axial images were reconstructed at 10% intervals across the cardiac cycle (0 to 90% of the RR). Effective dose length product was estimated to be between 200 and 500

mGy*cm. Ventricular volumes such as right ventricular end-diastolic volume (RVEDV), end-systolic volume (RVESV), and stroke volume (SV), and ejection fraction (RVEF) were obtained from volumes spanning one cardiac cycle as described below.

3.3.3 RV blood pool segmentation

Delineation of the RV blood pool to extract endocardial surfaces was performed using a U-Net based deep learning framework that has been previously shown to accurately segment blood chambers in cardiac CT angiograms[72]. The neural network was trained and validated on segmentations semi-automatically generated for end-systolic and end-diastolic frames for each patient. More information about this deep learning approach is available in Section 2.3.3. Segmentations generated by the deep learning approach were visually inspected to verify that segmented blood volumes were anatomically correct and temporally consistent.

3.3.4 Free and Septal Wall Function

Localized strain was calculated using a method called Stretch Quantification of Endocardial Engraved Zones (SQUEEZ)[95], which extracts the endocardial boundary of the RV as a mesh and uses point-cloud registration to obtain 3D displacement fields across the cardiac cycle. For any triangulation, x, from the mesh at any timepoint during the cardiac cycle, t, the regional shortening (RS_{CT}) is based on the changing area of the triangular mesh defined as the following:

$$\mathrm{RS_{CT}}(\mathrm{x},\mathrm{t}) = \sqrt{\frac{Area(x,t)}{Area(x,ED)}} - 1$$

Using this method, areas that are contracting will be negative and areas that are expanding will be positive. Regional shortening is reported as the maximum regional shortening (minimum value) over the cardiac cycle. Shortening in the free and septal walls was analyzed separately from the ventricular meshes. Attachment of the right ventricular wall to the left ventricle was used to separate the septum and right ventricular free wall[96]. Triangulations in the most basal and apex parts of the RV were excluded from free wall and septal delineation. Free and septal wall strain were then recorded as the average regional shortening at end systole for the entire free and septal wall areas respectively. RV discordance is defined the difference between the free wall strain and septal wall strain.

3.3.5 Comparison to Loading Conditions

Free and septal wall strain were compared between patients with heart failure and controls. In patients with and without heart failure, free wall and septal wall strain were compared against each other as well as with RVEDVI, an estimate of RV preload, in patients with and without heart failure. Free and septal wall strain were also compared to mPAP, an estimate of RV afterload. Due to the lack of right heart catheterization in the control cohort, control patients are displayed visually using the mean and standard deviation of the strain and clinically average mPAP values (14±3 mmHg)[97]. The difference between free and septal wall strain as a function of preload and afterload are reported as well.

3.3.6 Dyssynchrony Analysis

Contractions between the free and septal walls were analyzed for dyssynchrony. Dyssynchrony was calculated as the temporal difference between maximum septal contraction

and maximum free wall contraction. The temporal differences are expressed as %RR or percent of the cardiac cycle. Patients were found to have noticeable dyssynchronous contracting walls if the contractions between the free wall and septal wall occurred more than 10% of the cardiac cycle apart. For example, a patient would be found dyssynchronous if the free wall experienced peak strain 30% of the way through the cardiac cycle and the septal wall experienced peak strain at 40% of the way through the cardiac cycle or later. The synchrony of the total patient population was analyzed by analyzing the correlation between the time of free wall max strain and septal wall max strain.

3.3.7 Relationship to RV Failure after LVAD Implantation

The ability of loading conditions, free wall strain, septal wall strain, and the difference between free and septal wall strain to predict postoperative right ventricular failure was compared in a subset of patients who had left ventricular assist device (LVAD) implanted after CT and hemodynamic evaluation.

3.3.8 Statistical Analysis

Continuous variables are reported as mean ± standard deviation or median (interquartile range) for non-normally distributed data. Samples were compared using a two-sample Student's t-test. Correlation analysis is performed using the Pearson correlation coefficient. Correlations greater than 0.7 were considered strongly correlated, less than 0.7 but greater than 0.5 moderately correlated, and less than 0.5 mildly correlated. The receiver operator characteristic (ROC) curves were used to determine the optimal cutoff value of RV function indices for the

detection of poor outcomes. Statistical analyses were performed using Matlab. Two-sided P-values <0.05 were considered statistically significant.

3.4 Results

3.4.1 Patient Population

53 heart failure patients had CT scanning as part of work-up for advanced therapies. This was compared to 8 non-heart failure patients who had CT scanning. Demographics of the heart failure patients and controls are described in Table 3.1. Of the 53 patients, 17 went on to have LVAD implantation. Of those 8 (47%) went on to have right ventricular failure.

3.4.2 Free Wall and Septal Wall Function

As shown in Figure 3.1, absolute free wall function was decreased in heart failure patients compared to control patient (-0.14 ± 0.06 vs -0.23 ± 0.04, p = 0.002). Septal wall function was also impaired in heart failure patients compared to control patient (-0.12 ± 0.05 vs -0.24 ± 0.05, p < 0.001). The difference between free wall and septal wall function was more pronounced for heart failure patients than control patients (-0.018 ± 0.05 vs 0.016 ± 0.03, p = 0.048). Free wall and septal wall function were moderately correlated for heart failure patients (ρ= 0.65, p < 0.001, R2 = 0.42) and highly correlated for controls (ρ = 0.76, p = 0.03, R2 = 0.58).

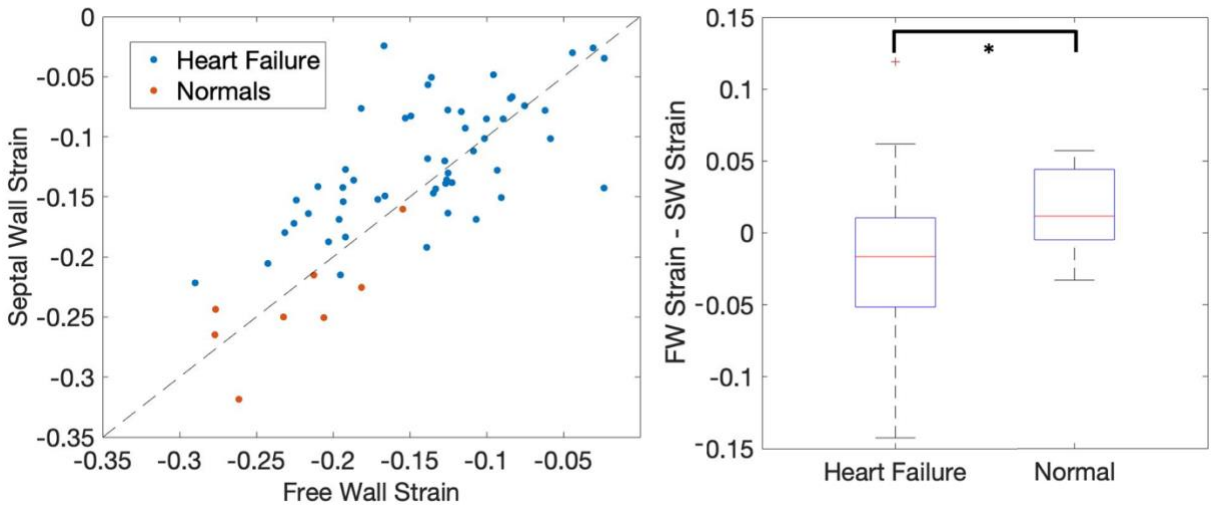

Figure 3.1 Comparison of free wall and septal wall strain between heart failure and non-heart failure patients. Left: Absolute free wall function was decreased in heart failure patients compared to control patients ($p = 0.002$). Absolute septal wall function was decreased in heart failure patients compared to control patients ($p < 0.001$). Right: The difference between free wall and septal wall function was more pronounced for heart failure patients than normal patients ($p = 0.048$).

3.4.3 Comparison with Loading Conditions

RVEDVI was moderately correlated with free wall strain ($\rho = 0.54$, $p < 0.001$, $R^2 = 0.35$) and mildly correlated with septal wall strain ($\rho = 0.43$, $p = 0.002$, $R^2 = 0.31$). mPAP was mildly correlated to FW strain ($\rho = 0.48$, $p < 0.001$, $R^2 = 0.24$), and septal wall strain ($\rho = 0.42$, $p = 0.002$, R2 = 0.18). mPAP and RVEDVI were uncorrelated to the RV discordance ($\rho = 0.29$ and $p = 0.71$, respectively). Neither mPAP nor RV EDVI were strongly predictive of regional strain ($R^2 < 0.4$). Notably, free wall strain had a stronger correlation with RV specific parameter, EDVI, than septal wall strain ($\rho = 0.54$ vs $\rho = 0.43$).

Additionally, RV Free wall strain was moderately correlated with RVEF ($\rho = -0.68$, $p < 0.001$, $R^2 = 0.46$) and mildly correlated with LVEF ($\rho = -0.45$, $p < 0.002$, $R^2 = 0.20$). Septal wall strain was almost equally correlated with LVEF ($\rho = -0.53$, $p < 0.001$, $R^2 = 0.28$) and RVEF ($\rho = -0.54$, $p < 0.001$, $R^2 = 0.29$).

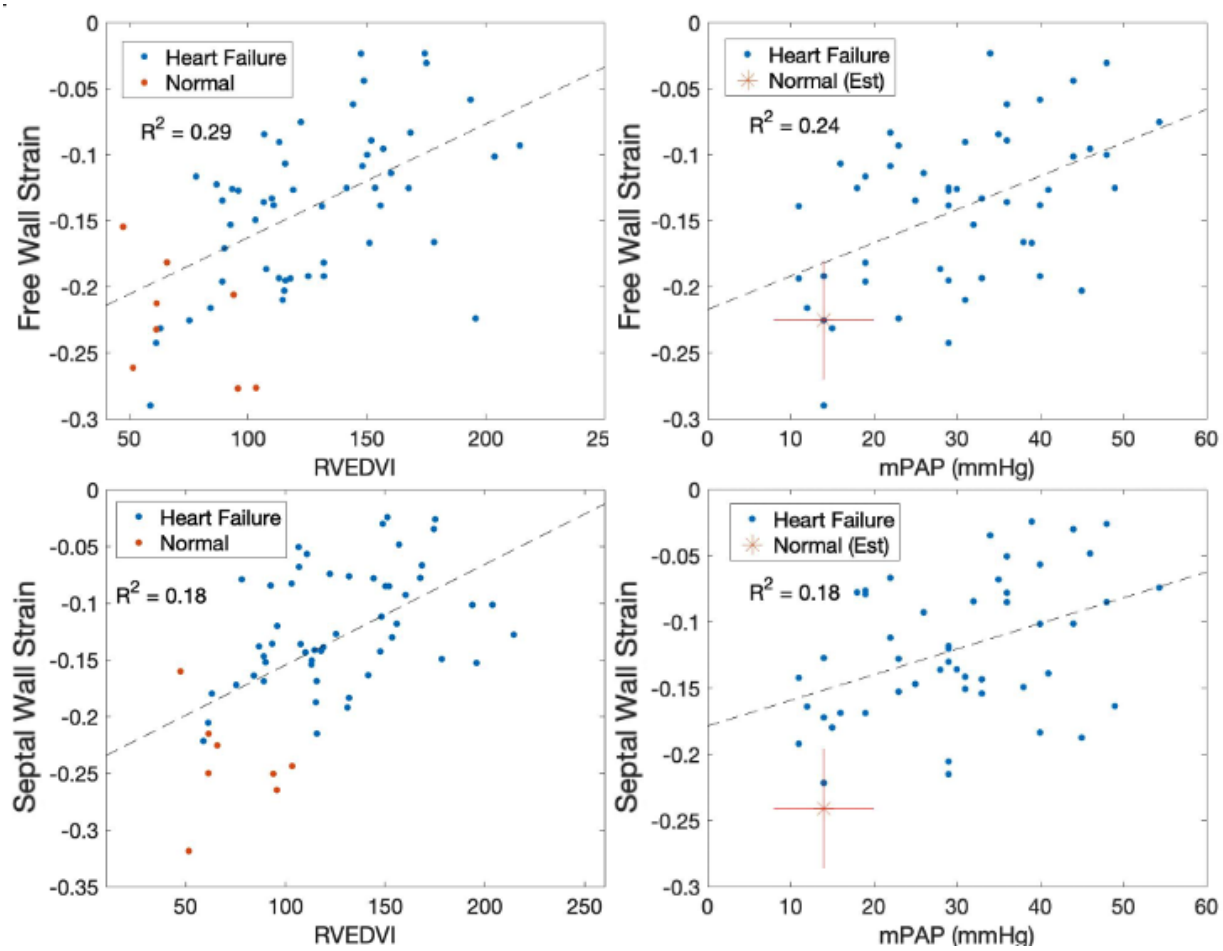

Figure 3.2 Effect of Loading Conditions on Regional RV Function - Comparison of Free wall function (left column) and septal wall function (right column) with preload (top row) and afterload (bottom row). Best fit lines are fit to heart failure patients. Control patients are shown for comparison.

Free wall, septal wall, and RV discordance predicted post-operative RVF with area-under-the curve (AUC) of receiver operating-characteristic (ROC) curve of 0.69 (95% CI:0.43-0.95), 0.67 (95% CI: 0.40 – 0.94), and 0.82 (95%CI: 0.61 – 1.00), respectively. Of these, prediction of post-operative RVF from RV discordance was found to be statistically significant (p=0.036).

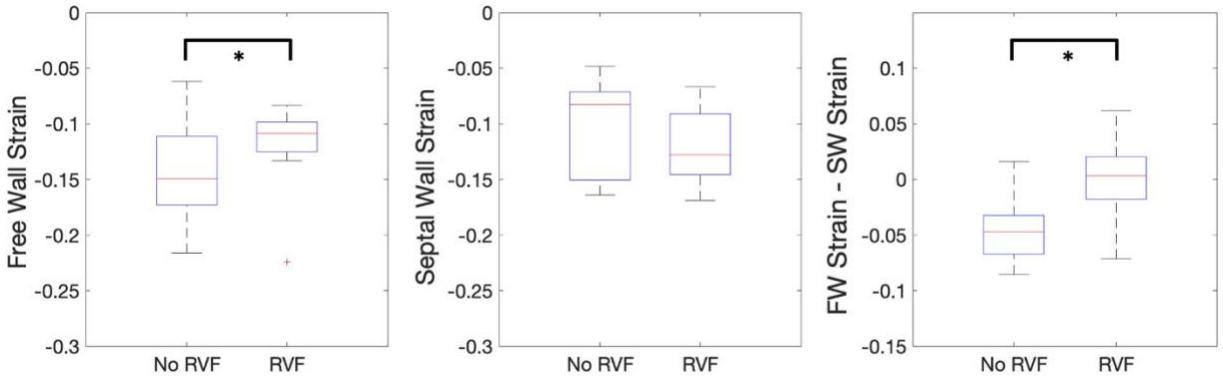

Figure 3.3 Comparison of Regional RV Function in RVF patients - Patients who went on to have postoperative RV failure had smaller free wall strain ($p<0.001$), similar septal wall strain, and significantly less difference in free and septal wall function ($p<0.001$).

3.4.4 Dyssynchrony between FW and SW Function

Dyssynchrony was not common in this patient population. Of the 53 patients analyzed, only 1 (2%) had observable dyssynchrony between the free wall and septal wall. For the patient population, the median difference between the free wall and septal wall contraction was 0±5 %RR i.e. simultaneous contraction. For the whole patient population, %RR at free wall max strain was highly correlated with %RR at septal wall max strain ($\rho = 0.98$, $p < 0.001$, $R^2 = 0.96$).

3.4.4 Association with RV Failure

AUC of RV FW strain, SW strain, RV discordance, and RVEDVI are shown in Figure 3.4. RV discordance performed similarly to RVEDVI (0.75, 95% CI: 0.61 – 1,). Neither mPAP (0.64, 95% CI: 0.42 – 0.86) nor RVEF (0.55, 95% CI: 0.32 – 0.78) where significant predictors of RVF.

3.5 Discussion

In heart failure patients, we observed impairment in both free and septal wall strain, and that free wall strain was more pronounced than septal wall strain in heart failure patients. Since the septal wall is shared between ventricles and the free wall is unique to the right ventricle, the discordance or difference, may reflect free wall compensation in response to LV dysfunction. As such, RV discordance may provide additional benefit for RV analysis by placing free wall strain in context of LV function.

Analyzing the relationship between EDVI and RV discordance, we observed an absence of patients with both high strain (RS_{CT} < -0.2) and RV enlargement (RVEDVI > 150ml/m2). This suggests that high free wall strain may protect against RV enlargement, a risk factor for RV failure. This is further supported by the findings that in the subset of patients who went on have LVAD implantation, non-RV failure patients had significantly better free wall function than septal wall function while RV failure patients had similar free wall and septal wall function (Figure 3.3).

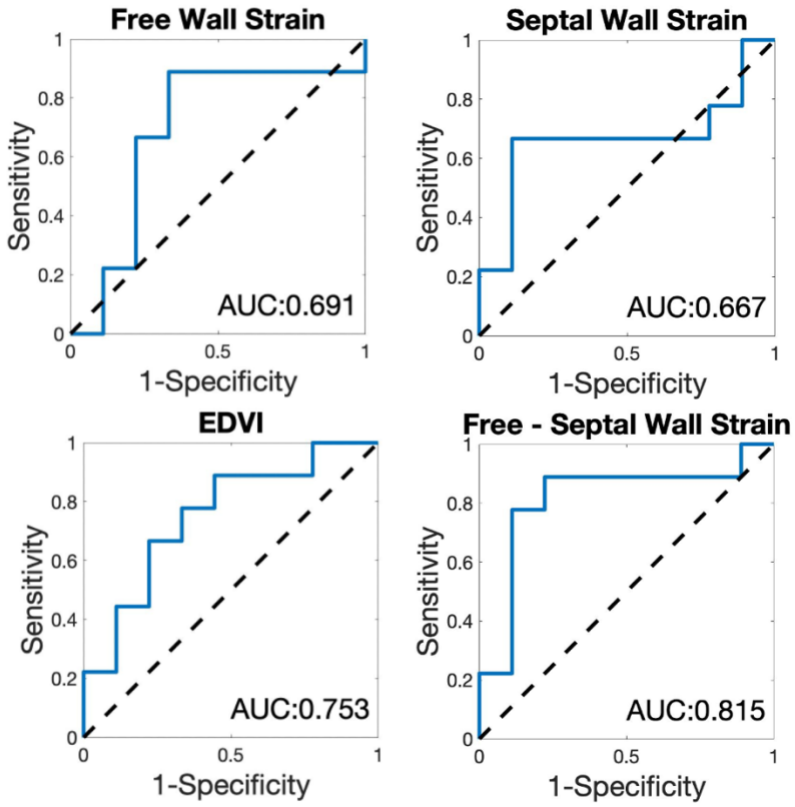

Figure 3.4 Ability of Regional Strain to Predict post LVAD RV Failure - Free wall, septal wall, and relative free wall function were able to predict post-operative RVF similarly to the late marker of dysfunction, RVEDVI. Further, the difference between free and septal wall strain improved the predictive ability of regional strain.

RV free and septal wall strains were only mildly correlated ($\rho < 0.5$) with preoperative mPAP and septal wall strain was mildly correlated with RV EDVI. Free wall strain and EDVI had a significant but moderate correlation ($\rho = 0.54$, $p < 0.001$) as expected from the Frank-Starling Law. This suggests that free and septal wall strain metrics cannot be fully explained by these tested loading conditions.

To date, this study is the first to analyze free wall and septal wall strain using cineCT for this population. While 2D echocardiography is clinically used to measure FW and SW RV strain, CT may confer some benefits for this population. Namely, CT is not limited by severe RV enlargement, which leads to poor image quality in echocardiography. This, in turn, led to a low

rate of data exclusion in CT studies. In our study, all included patients scanned were successfully analyzed. Further, CT is not affected by angle of acquisition and is inherently a 3D acquisition.

Our findings that free wall strain is a significant predictor of RVF broadly agree with similar studies that use 2D speckle tracking echo to determine right ventricular free wall and septal wall strain [98]. Magunia et al was the first group to analyze 3D free wall echo strain in patients undergoing LVAD implantation [51]. They found 3D free wall strain to have the strongest discriminative capability of both RVF and mid-term survival in a cohort of 26 patients. Additionally, in patients with heart failure with preserved ejection fraction (HFpEF), Meng et al found that 3D echo strain of the RV FW to be a powerful predictor of poor outcomes [99].

This study has some limitations. Namely, this was a retrospective, single center analysis of a limited group of patients, which may affect the generalizability of these results. Further, due to the low number of patients who went on to have an LVAD implantation, multivariate analysis for RVF outcomes was precluded. Additionally due to the study size, the ability of free wall and septal wall strain difference would need to be validated in a larger cohort. While cineCT does have some advantages over speckle-tracking echo, it also carries risks such as radiation exposure and nephrotoxicity from the use of contrast agent for patients with poor renal function. Lastly, while we found these results to be significant by themselves, there was no comparison with speckle-tracking echocardiographic strain.

3.5 Conclusion

Right ventricular free wall and septal wall strain can be measured using cineCT. These measures of regional function can help identify signs of early RV dysfunction in heart failure. These measures are not well explained by loading conditions (pre-operative pulmonary pressure and

end diastolic volume). Free wall and septal wall strain may then be used to separate patients into a low-risk phenotype with preserved volume and strong FW function, intermediate risk with enlarged volume and strong FW function, and high risk with enlarged volume and weak FW function.

3.6 Acknowledgement

Chapter 3, in part, is currently being prepared for submission for publication of the material as "Free and Septal Wall Function for Risk Assessment in Heart Failure using Computed Tomography" by Anderson Scott, Zhennong Chen, Seth Kligerman, Paul Kim, Hao Tran, Eric Adler, and Francisco Contijoch. The dissertation author is the primary investigator and will be first author of this manuscript.

REFERENCES

1. Ambrosy AP, Fonarow GC, Butler J, Chioncel O, Greene SJ, Vaduganathan M, Nodari S, Lam CSP, Sato N, Shah AN, Gheorghiade M (2014) The Global Health and Economic Burden of Hospitalizations for Heart Failure. Journal of the American College of Cardiology 63:1123–1133. https://doi.org/10.1016/j.jacc.2013.11.053

2. Roger VL (2013) Epidemiology of Heart Failure. Circ Res 113:646–659. https://doi.org/10.1161/CIRCRESAHA.113.300268

3. Cook JL, Grady KL, Colvin M, Joseph SM, Brisco MA, Walsh MN (2015) Sex Differences in the Care of Patients With Advanced Heart Failure. Circ: Cardiovascular Quality and Outcomes 8:. https://doi.org/10.1161/CIRCOUTCOMES.115.001730

4. Choi H-M, Park M-S, Youn J-C (2019) Update on heart failure management and future directions. Korean J Intern Med 34:11–43. https://doi.org/10.3904/kjim.2018.428

5. Dunlay SM, Roger VL, Redfield MM (2017) Epidemiology of heart failure with preserved ejection fraction. Nat Rev Cardiol 14:591–602. https://doi.org/10.1038/nrcardio.2017.65

6. Gude E, Fiane AE (2021) Can mechanical circulatory support be an effective treatment for HFpEF patients? Heart Fail Rev. https://doi.org/10.1007/s10741-021-10154-1

7. Kormos RL, Cowger J, Pagani FD, Teuteberg JJ, Goldstein DJ, Jacobs JP, Higgins RS, Stevenson LW, Stehlik J, Atluri P, Grady KL, Kirklin JK (2019) The Society of Thoracic Surgeons Intermacs database annual report: Evolving indications, outcomes, and scientific partnerships. The Journal of Heart and Lung Transplantation 38:114–126. https://doi.org/10.1016/j.healun.2018.11.013

8. de By TMMH, Mohacsi P, Gahl B, Zittermann A, Krabatsch T, Gustafsson F, Leprince P, Meyns B, Netuka I, Caliskan K, Castedo E, Musumeci F, Vincentelli A, Hetzer R, Gummert J, the EUROMACS members (2018) The European Registry for Patients with Mechanical Circulatory Support (EUROMACS) of the European Association for Cardio-Thoracic Surgery (EACTS): second report. European Journal of Cardio-Thoracic Surgery 53:309–316. https://doi.org/10.1093/ejcts/ezx320

9. Nakatani T, Sase K, Oshiyama H, Akiyama M, Horie M, Nawata K, Nishinaka T, Tanoue Y, Toda K, Tozawa M, Yamazaki S, Yanase M, Ohtsu H, Ishida M, Hiramatsu A, Ishii K, Kitamura S (2017) Japanese registry for Mechanically Assisted Circulatory Support: First report. The Journal of Heart and Lung Transplantation 36:1087–1096. https://doi.org/10.1016/j.healun.2017.08.002

10. Levine A, Gass A (2019) Third-Generation LVADs: Has Anything Changed? Cardiology in Review 27:293–301. https://doi.org/10.1097/CRD.0000000000000268

11. Stevenson LW, Pagani FD, Young JB, Jessup M, Miller L, Kormos RL, Naftel DC, Ulisney K, Desvigne-Nickens P, Kirklin JK (2009) INTERMACS Profiles of Advanced Heart

Failure: The Current Picture. The Journal of Heart and Lung Transplantation 28:535–541. https://doi.org/10.1016/j.healun.2009.02.015

12. Bowen RES, Graetz TJ, Emmert DA, Avidan MS (2020) Statistics of heart failure and mechanical circulatory support in 2020. Ann Transl Med 8:827–827. https://doi.org/10.21037/atm-20-1127

13. Khush KK, Cherikh WS, Chambers DC, Harhay MO, Hayes D, Hsich E, Meiser B, Potena L, Robinson A, Rossano JW, Sadavarte A, Singh TP, Zuckermann A, Stehlik J (2019) The International Thoracic Organ Transplant Registry of the International Society for Heart and Lung Transplantation: Thirty-sixth adult heart transplantation report — 2019; focus theme: Donor and recipient size match. The Journal of Heart and Lung Transplantation 38:1056–1066. https://doi.org/10.1016/j.healun.2019.08.004

14. Flint KM, Spertus JA, Tang F, Jones P, Fendler TJ, Allen LA (2017) Association of global and disease-specific health status with outcomes following continuous-flow left ventricular assist device implantation. BMC Cardiovasc Disord 17:78. https://doi.org/10.1186/s12872-017-0510-9

15. Farré N, Vela E, Clèries M, Bustins M, Cainzos-Achirica M, Enjuanes C, Moliner P, Ruiz S, Verdú-Rotellar JM, Comín-Colet J (2017) Real world heart failure epidemiology and outcome: A population-based analysis of 88,195 patients. PLoS ONE 12:e0172745. https://doi.org/10.1371/journal.pone.0172745

16. Basir MB, Schreiber TL, Grines CL, Dixon SR, Moses JW, Maini BS, Khandelwal AK, Ohman EM, O'Neill WW (2017) Effect of Early Initiation of Mechanical Circulatory Support on Survival in Cardiogenic Shock. The American Journal of Cardiology 119:845–851. https://doi.org/10.1016/j.amjcard.2016.11.037

17. Slaughter MS, Rogers JG, Milano CA, Russell SD, Conte JV, Feldman D, Sun B, Tatooles AJ, Delgado RM, Long JW, Wozniak TC, Ghumman W, Farrar DJ, Frazier OH (2009) Advanced Heart Failure Treated with Continuous-Flow Left Ventricular Assist Device. N Engl J Med 361:2241–2251. https://doi.org/10.1056/NEJMoa0909938

18. Rogers JG, Aaronson KD, Boyle AJ, Russell SD, Milano CA, Pagani FD, Edwards BS, Park S, John R, Conte JV, Farrar DJ, Slaughter MS (2010) Continuous Flow Left Ventricular Assist Device Improves Functional Capacity and Quality of Life of Advanced Heart Failure Patients. Journal of the American College of Cardiology 55:1826–1834. https://doi.org/10.1016/j.jacc.2009.12.052

19. Kirklin JK, Pagani FD, Kormos RL, Stevenson LW, Blume ED, Myers SL, Miller MA, Baldwin JT, Young JB, Naftel DC (2017) Eighth annual INTERMACS report: Special focus on framing the impact of adverse events. The Journal of Heart and Lung Transplantation 36:1080–1086. https://doi.org/10.1016/j.healun.2017.07.005

20. LaRue SJ, Raymer DS, Pierce BR, Nassif ME, Sparrow CT, Vader JM (2017) Clinical outcomes associated with INTERMACS-defined right heart failure after left ventricular

assist device implantation. J Heart Lung Transplant 36:475–477. https://doi.org/10.1016/j.healun.2016.12.017

21. Kirklin JK, Xie R, Cowger J, de By TMMH, Nakatani T, Schueler S, Taylor R, Lannon J, Mohacsi P, Gummert J, Goldstein D, Caliskan K, Hannan MM (2018) Second annual report from the ISHLT Mechanically Assisted Circulatory Support Registry. The Journal of Heart and Lung Transplantation 37:685–691. https://doi.org/10.1016/j.healun.2018.01.1294

22. Holman WL (2012) Interagency Registry for Mechanically Assisted Circulatory Support (INTERMACS): What Have We Learned and What Will We Learn? Circulation 126:1401–1406. https://doi.org/10.1161/CIRCULATIONAHA.112.097816

23. Lampert BC, Teuteberg JJ (2015) Right ventricular failure after left ventricular assist devices. The Journal of Heart and Lung Transplantation 34:1123–1130. https://doi.org/10.1016/j.healun.2015.06.015

24. Genovese EA, Dew MA, Teuteberg JJ, Simon MA, Kay J, Siegenthaler MP, Bhama JK, Bermudez CA, Lockard KL, Winowich S, Kormos RL (2009) Incidence and Patterns of Adverse Event Onset During the First 60 Days After Ventricular Assist Device Implantation. The Annals of Thoracic Surgery 88:1162–1170. https://doi.org/10.1016/j.athoracsur.2009.06.028

25. Alba AC, Agoritsas T, Walsh M, Hanna S, Iorio A, Devereaux PJ, McGinn T, Guyatt G (2017) Discrimination and Calibration of Clinical Prediction Models: Users' Guides to the Medical Literature. JAMA 318:1377. https://doi.org/10.1001/jama.2017.12126

26. Frankfurter C, Molinero M, Vishram-Nielsen JKK, Foroutan F, Mak S, Rao V, Billia F, Orchanian-Cheff A, Alba AC (2020) Predicting the Risk of Right Ventricular Failure in Patients Undergoing Left Ventricular Assist Device Implantation: A Systematic Review. Circ: Heart Failure 13:. https://doi.org/10.1161/CIRCHEARTFAILURE.120.006994

27. Bellavia D, Iacovoni A, Scardulla C, Moja L, Pilato M, Kushwaha SS, Senni M, Clemenza F, Agnese V, Falletta C, Romano G, Maalouf J, Dandel M (2017) Prediction of right ventricular failure after ventricular assist device implant: systematic review and meta-analysis of observational studies: Meta-analysis of right ventricular failure determinants after LVAD implant. Eur J Heart Fail 19:926–946. https://doi.org/10.1002/ejhf.733

28. Argiriou M, Kolokotron S-M, Sakellaridis T, Argiriou O, Charitos C, Zarogoulidis P, Katsikogiannis N, Kougioumtzi I, Machairiotis N, Tsiouda T, Tsakiridis K, Zarogoulidis K (2014) Right heart failure post left ventricular assist device implantation. J Thorac Dis 6 Suppl 1:S52-59. https://doi.org/10.3978/j.issn.2072-1439.2013.10.26

29. Soliman OII, Akin S, Muslem R, Boersma E, Manintveld OC, Krabatsch T, Gummert JF, de By TMMH, Bogers AJJC, Zijlstra F, Mohacsi P, Caliskan K (2018) Derivation and Validation of a Novel Right-Sided Heart Failure Model After Implantation of Continuous Flow Left Ventricular Assist Devices: The EUROMACS (European Registry for Patients with Mechanical Circulatory Support) Right-Sided Heart Failure Risk Score. Circulation 137:891–906. https://doi.org/10.1161/CIRCULATIONAHA.117.030543

30. Rigolin VH, Robiolio PA, Wilson JS, Harrison JK, Bashore TM (1995) The forgotten chamber: The importance of the right ventricle. Cathet Cardiovasc Diagn 35:18–28. https://doi.org/10.1002/ccd.1810350105

31. Voelkel NF, Quaife RA, Leinwand LA, Barst RJ, McGoon MD, Meldrum DR, Dupuis J, Long CS, Rubin LJ, Smart FW, Suzuki YJ, Gladwin M, Denholm EM, Gail DB (2006) Right Ventricular Function and Failure: Report of a National Heart, Lung, and Blood Institute Working Group on Cellular and Molecular Mechanisms of Right Heart Failure. Circulation 114:1883–1891. https://doi.org/10.1161/CIRCULATIONAHA.106.632208

32. Kukulski T, Hübbert L, Arnold M, Wranne B, Hatle L, Sutherland GR (2000) Normal Regional Right Ventricular Function and Its Change with Age: A Doppler Myocardial Imaging Study. Journal of the American Society of Echocardiography 13:194–204. https://doi.org/10.1067/mje.2000.103106

33. Naeije R, Brimioulle S, Dewachter L (2014) Biomechanics of the Right Ventricle in Health and Disease (2013 Grover Conference Series). Pulm circ 4:395–406. https://doi.org/10.1086/677354

34. Setaro JF, Cleman MW, Remetz MS (1992) The right ventricle in disorders causing pulmonary venous hypertension. Cardiol Clin 10:165–183

35. Klima UP, Guerrero JL, Vlahakes GJ (1999) Myocardial perfusion and right ventricular function. Ann Thorac Cardiovasc Surg 5:74–80

36. Meyer P, Filippatos GS, Ahmed MI, Iskandrian AE, Bittner V, Perry GJ, White M, Aban IB, Mujib M, Dell'Italia LJ, Ahmed A (2010) Effects of Right Ventricular Ejection Fraction on Outcomes in Chronic Systolic Heart Failure. Circulation 121:252–258. https://doi.org/10.1161/CIRCULATIONAHA.109.887570

37. Polak JF, Holman BL, Wynne J, Colucci WS (1983) Right ventricular ejection fraction: An indicator of increased mortality in patients with congestive heart failure associated with coronary artery disease. Journal of the American College of Cardiology 2:217–224. https://doi.org/10.1016/S0735-1097(83)80156-9

38. Shah PK, Maddahi J, Staniloff HM, Ellrodt AG, Pichler M, Swan HJC, Berman DS (1986) Variable spectrum and prognostic implications of left and right ventricular ejection fractions in patients with and without clinical heart failure after acute myocardial infarction. The American Journal of Cardiology 58:387–393. https://doi.org/10.1016/0002-9149(86)90001-9

39. Karatasakis GT, Karagounis LA, Kalyvas PA, Manginas A, Athanassopoulos GD, Aggelakas SA, Cokkinos DV (1998) Prognostic significance of echocardiographically estimated right ventricular shortening in advanced heart failure. The American Journal of Cardiology 82:329–334. https://doi.org/10.1016/S0002-9149(98)00344-0

40. Greiner S, André F, Heimisch M, Aurich M, Steen H, Katus HA, Mereles D (2019) A closer look at right ventricular 3D volume quantification by transthoracic echocardiography and

cardiac MRI. Clinical Radiology 74:490.e7-490.e14. https://doi.org/10.1016/j.crad.2019.03.005

41. Aziz W, Claridge S, Ntalas I, Gould J, Vecchi A, Razeghi O, Toth D, Mountney P, Preston R, Rinaldi CA, Razavi R, Niederer S, Rajani R (2019) Emerging role of cardiac computed tomography in heart failure. ESC Heart Failure 6:909–920. https://doi.org/10.1002/ehf2.12479

42. Kim JY, Suh YJ, Han K, Kim YJ, Choi BW (2020) Cardiac CT for Measurement of Right Ventricular Volume and Function in Comparison with Cardiac MRI: A Meta-Analysis. Korean J Radiol 21:450. https://doi.org/10.3348/kjr.2019.0499

43. Burkhoff D, Mirsky I, Suga H (2005) Assessment of systolic and diastolic ventricular properties via pressure-volume analysis: a guide for clinical, translational, and basic researchers. American Journal of Physiology-Heart and Circulatory Physiology 289:H501–H512. https://doi.org/10.1152/ajpheart.00138.2005

44. Mohamed A, Mehta N, Eisen HJ (2017) New role of mechanical assist device as bridge to transplant: USA perspective. Current Opinion in Organ Transplantation 22:231–235. https://doi.org/10.1097/MOT.0000000000000418

45. Dang N, Topkara V, Mercando M, Kay J, Kruger K, Aboodi M, Oz M, Naka Y (2006) Right Heart Failure After Left Ventricular Assist Device Implantation in Patients With Chronic Congestive Heart Failure. The Journal of Heart and Lung Transplantation 25:1–6. https://doi.org/10.1016/j.healun.2005.07.008

46. Matthews JC, Koelling TM, Pagani FD, Aaronson KD (2008) The Right Ventricular Failure Risk Score. Journal of the American College of Cardiology 51:2163–2172. https://doi.org/10.1016/j.jacc.2008.03.009

47. Fitzpatrick JR, Frederick JR, Hsu VM, Kozin ED, O'Hara ML, Howell E, Dougherty D, McCormick RC, Laporte CA, Cohen JE, Southerland KW, Howard JL, Jessup ML, Morris RJ, Acker MA, Woo YJ (2008) Risk Score Derived from Pre-operative Data Analysis Predicts the Need for Biventricular Mechanical Circulatory Support. The Journal of Heart and Lung Transplantation 27:1286–1292. https://doi.org/10.1016/j.healun.2008.09.006

48. Aymami M, Amsallem M, Adams J, Sallam K, Moneghetti K, Wheeler M, Hiesinger W, Teuteberg J, Weisshaar D, Verhoye J-P, Woo YJ, Ha R, Haddad F, Banerjee D (2018) The Incremental Value of Right Ventricular Size and Strain in the Risk Assessment of Right Heart Failure Post - Left Ventricular Assist Device Implantation. J Card Fail 24:823–832. https://doi.org/10.1016/j.cardfail.2018.10.012

49. Wu VC-C, Takeuchi M (2018) Echocardiographic assessment of right ventricular systolic function. Cardiovasc Diagn Ther 8:70–79. https://doi.org/10.21037/cdt.2017.06.05

50. Kiernan MS, French AL, DeNofrio D, Parmar YJ, Pham DT, Kapur NK, Pandian NG, Patel AR (2015) Preoperative three-dimensional echocardiography to assess risk of right

ventricular failure after left ventricular assist device surgery. J Card Fail 21:189–197. https://doi.org/10.1016/j.cardfail.2014.12.009

51. Magunia H, Dietrich C, Langer HF, Schibilsky D, Schlensak C, Rosenberger P, Nowak-Machen M (2018) 3D echocardiography derived right ventricular function is associated with right ventricular failure and mid-term survival after left ventricular assist device implantation. Int J Cardiol 272:348–355. https://doi.org/10.1016/j.ijcard.2018.06.026

52. Otten A, Kurz S, Anwar S, Potapov E, Krall C, O'Brien B, Habazettl H, Krabatsch T, Kukucka M (2018) Prognostic value of 3-dimensional echocardiographical heart volume assessment in patients scheduled for left ventricular assist device implantation. European Journal of Cardio-Thoracic Surgery 54:169–175. https://doi.org/10.1093/ejcts/ezy002

53. Addetia K, Muraru D, Badano LP, Lang RM (2019) New Directions in Right Ventricular Assessment Using 3-Dimensional Echocardiography. JAMA Cardiol 4:936. https://doi.org/10.1001/jamacardio.2019.2424

54. Kang G, Ha R, Banerjee D (2016) Pulmonary artery pulsatility index predicts right ventricular failure after left ventricular assist device implantation. The Journal of Heart and Lung Transplantation 35:67–73. https://doi.org/10.1016/j.healun.2015.06.009

55. Morine KJ, Kiernan MS, Pham DT, Paruchuri V, Denofrio D, Kapur NK (2016) Pulmonary Artery Pulsatility Index Is Associated With Right Ventricular Failure After Left Ventricular Assist Device Surgery. Journal of Cardiac Failure 22:110–116. https://doi.org/10.1016/j.cardfail.2015.10.019

56. Raymer DS, Moreno JD, Sintek MA, Nassif ME, Sparrow CT, Adamo L, Novak EL, LaRue SJ, Vader JM (2019) The Combination of Tricuspid Annular Plane Systolic Excursion and HeartMate Risk Score Predicts Right Ventricular Failure After Left Ventricular Assist Device Implantation. ASAIO Journal 65:247–251. https://doi.org/10.1097/MAT.0000000000000808

57. Acharya D, Aryal S, Loyaga-Rendon R, Pamboukian SV, Tallaj J, Kirklin JK, Holman WL, Singh S (2019) Use of Computed Tomography in Preoperative Planning for Heartware Left Ventricular Assist Device Placement. ASAIO Journal 65:70–76. https://doi.org/10.1097/MAT.0000000000000761

58. Interagency Registry for Mechanically Assisted Circulatory Support Appendix A - adverse event definitions

59. Hanley JA, McNeil BJ (1982) The meaning and use of the area under a receiver operating characteristic (ROC) curve. Radiology 143:29–36. https://doi.org/10.1148/radiology.143.1.7063747

60. Drakos SG, Janicki L, Horne BD, Kfoury AG, Reid BB, Clayson S, Horton K, Haddad F, Li DY, Renlund DG, Fisher PW (2010) Risk Factors Predictive of Right Ventricular Failure After Left Ventricular Assist Device Implantation. The American Journal of Cardiology 105:1030–1035. https://doi.org/10.1016/j.amjcard.2009.11.026

61. Monitillo F, Di Terlizzi V, Gioia MI, Barone R, Grande D, Parisi G, Brunetti ND, Iacoviello M (2020) Right Ventricular Function in Chronic Heart Failure: From the Diagnosis to the Therapeutic Approach. JCDD 7:12. https://doi.org/10.3390/jcdd7020012

62. de Groote P, Millaire A, Foucher-Hossein C, Nugue O, Marchandise X, Ducloux G, Lablanche J-M (1998) Right ventricular ejection fraction is an independent predictor of survival in patients with moderate heart failure. Journal of the American College of Cardiology 32:948–954. https://doi.org/10.1016/S0735-1097(98)00337-4

63. Aschauer S, Kammerlander AA, Zotter-Tufaro C, Ristl R, Pfaffenberger S, Bachmann A, Duca F, Marzluf BA, Bonderman D, Mascherbauer J (2016) The right heart in heart failure with preserved ejection fraction: insights from cardiac magnetic resonance imaging and invasive haemodynamics: The right heart in heart failure with preserved ejection fraction. Eur J Heart Fail 18:71–80. https://doi.org/10.1002/ejhf.418

64. Zornoff LAM, Skali H, Pfeffer MA, St. John Sutton M, Rouleau JL, Lamas GA, Plappert T, Rouleau JR, Moyé LA, Lewis SJ, Braunwald E, Solomon SD (2002) Right ventricular dysfunction and risk of heart failure and mortality after myocardial infarction. Journal of the American College of Cardiology 39:1450–1455. https://doi.org/10.1016/S0735-1097(02)01804-1

65. Ghio S, Gavazzi A, Campana C, Inserra C, Klersy C, Sebastiani R, Arbustini E, Recusani F, Tavazzi L (2001) Independent and additive prognostic value of right ventricular systolic function and pulmonary artery pressure in patients with chronic heart failure. Journal of the American College of Cardiology 37:183–188. https://doi.org/10.1016/S0735-1097(00)01102-5

66. Kormos RL, Teuteberg JJ, Pagani FD, Russell SD, John R, Miller LW, Massey T, Milano CA, Moazami N, Sundareswaran KS, Farrar DJ (2010) Right ventricular failure in patients with the HeartMate II continuous-flow left ventricular assist device: Incidence, risk factors, and effect on outcomes. The Journal of Thoracic and Cardiovascular Surgery 139:1316–1324. https://doi.org/10.1016/j.jtcvs.2009.11.020

67. Brener MI, Masoumi A, Ng VG, Tello K, Bastos MB, Cornwell WK, Hsu S, Tedford RJ, Lurz P, Rommel K-P, Kresoja K-P, Nagueh SF, Kanwar MK, Kapur NK, Hiremath G, Sarraf M, Van Den Enden AJM, Van Mieghem NM, Heerdt PM, Hahn RT, Kodali SK, Sayer GT, Uriel N, Burkhoff D (2022) Invasive Right Ventricular Pressure-Volume Analysis: Basic Principles, Clinical Applications, and Practical Recommendations. Circ: Heart Failure 15:e009101. https://doi.org/10.1161/CIRCHEARTFAILURE.121.009101

68. Scott A, Kligerman S, Hernandez DH, Kim P, Tran H, Pretorius V, Adler E, Contijoch F Preoperative Computed Tomography Assessment of Risk of Right Ventricle Failure After Left Ventricular Assist Device Placement. 7

69. Suga H, Hayashi T, Shirahata M (1981) Ventricular systolic pressure-volume area as predictor of cardiac oxygen consumption. American Journal of Physiology-Heart and Circulatory Physiology 240:H39–H44. https://doi.org/10.1152/ajpheart.1981.240.1.H39

70. Nozawa T, Yasumura Y, Futaki S, Tanaka N, Uenishi M, Suga H (1988) Efficiency of energy transfer from pressure-volume area to external mechanical work increases with contractile state and decreases with afterload in the left ventricle of the anesthetized closed-chest dog. Circulation 77:1116–1124. https://doi.org/10.1161/01.CIR.77.5.1116

71. Kormos RL, Antonides CFJ, Goldstein DJ, Cowger JA, Starling RC, Kirklin JK, Rame JE, Rosenthal D, Mooney ML, Caliskan K, Messe SR, Teuteberg JJ, Mohacsi P, Slaughter MS, Potapov EV, Rao V, Schima H, Stehlik J, Joseph S, Koenig SC, Pagani FD (2020) Updated definitions of adverse events for trials and registries of mechanical circulatory support: A consensus statement of the mechanical circulatory support academic research consortium. The Journal of Heart and Lung Transplantation 39:735–750. https://doi.org/10.1016/j.healun.2020.03.010

72. Chen Z, Rigolli M, Vigneault DM, Kligerman S, Hahn L, Narezkina A, Craine A, Lowe K, Contijoch F (2021) Automated cardiac volume assessment and cardiac long- and short-axis imaging plane prediction from electrocardiogram-gated computed tomography volumes enabled by deep learning. European Heart Journal - Digital Health 2:311–322. https://doi.org/10.1093/ehjdh/ztab033

73. Rohatgi A (2021) WebPlotDigitizer: Version 4.5

74. Suga H, Igarashi Y, Yamada O, Goto Y (1985) Mechanical efficiency of the left ventricle as a function of preload, afterload, and contractility. Heart Vessels 1:3–8. https://doi.org/10.1007/BF02066480

75. Vanderpool RR, Pinsky MR, Naeije R, Deible C, Kosaraju V, Bunner C, Mathier MA, Lacomis J, Champion HC, Simon MA (2015) RV-pulmonary arterial coupling predicts outcome in patients referred for pulmonary hypertension. Heart 101:37–43. https://doi.org/10.1136/heartjnl-2014-306142

76. Inuzuka R, Hsu S, Tedford RJ, Senzaki H (2018) Single-Beat Estimation of Right Ventricular Contractility and Its Coupling to Pulmonary Arterial Load in Patients With Pulmonary Hypertension. JAHA 7:. https://doi.org/10.1161/JAHA.117.007929

77. Opotowsky AR, Hess E, Maron BA, Brittain EL, Barón AE, Maddox TM, Alshawabkeh LI, Wertheim BM, Xu M, Assad TR, Rich JD, Choudhary G, Tedford RJ (2017) Thermodilution vs Estimated Fick Cardiac Output Measurement in Clinical Practice: An Analysis of Mortality From the Veterans Affairs Clinical Assessment, Reporting, and Tracking (VA CART) Program and Vanderbilt University. JAMA Cardiol 2:1090. https://doi.org/10.1001/jamacardio.2017.2945

78. Pereira A, Santos JG, Loureiro MJ, Ferreira F, Almeida AR, Cale R, Repolho D, Vitorino S, Morgado J, Pereira H (2020) Thermodilution vs indirect fick cardiac output measurement in clinical practice: insights from a tertiary centre. European Heart Journal 41:ehaa946.2252. https://doi.org/10.1093/ehjci/ehaa946.2252

79. Martin B, Jan P, Jan H (2002) Effect of the degree of tricuspid regurgitation on cardiac output measurements by thermodilution. Intensive Care Med 28:1117–1121. https://doi.org/10.1007/s00134-002-1352-0

80. Cigarroa RG, Lange RA, Williams RH, Bedotto JB, Hillis LD (1989) Underestimation of cardiac output by thermodilution in patients with tricuspid regurgitation. The American Journal of Medicine 86:417–420. https://doi.org/10.1016/0002-9343(89)90339-2

81. Heerdt PM, Blessios GA, Beach ML, Hogue CW (2001) Flow dependency of error in thermodilution measurement of cardiac output during acute tricuspid regurgitation. Journal of Cardiothoracic and Vascular Anesthesia 15:183–187. https://doi.org/10.1053/jcan.2001.21947

82. Crean AM, Maredia N, Ballard G, Menezes R, Wharton G, Forster J, Greenwood JP, Thomson JD (2011) 3D Echo systematically underestimates right ventricular volumes compared to cardiovascular magnetic resonance in adult congenital heart disease patients with moderate or severe RV dilatation. J Cardiovasc Magn Reson 13:78. https://doi.org/10.1186/1532-429X-13-78

83. Shimada YJ, Shiota M, Siegel RJ, Shiota T (2010) Accuracy of Right Ventricular Volumes and Function Determined by Three-Dimensional Echocardiography in Comparison with Magnetic Resonance Imaging: A Meta-Analysis Study. Journal of the American Society of Echocardiography 23:943–953. https://doi.org/10.1016/j.echo.2010.06.029

84. Khoo NS, Young A, Occleshaw C, Cowan B, Zeng ISL, Gentles TL (2009) Assessments of Right Ventricular Volume and Function Using Three-Dimensional Echocardiography in Older Children and Adults With Congenital Heart Disease: Comparison With Cardiac Magnetic Resonance Imaging. Journal of the American Society of Echocardiography 22:1279–1288. https://doi.org/10.1016/j.echo.2009.08.011

85. Suga H, Hayashi T, Shirahata M, Suehiro S, Hisano R (1981) Regression of cardiac oxygen consumption on ventricular pressure-volume area in dog. American Journal of Physiology-Heart and Circulatory Physiology 240:H320–H325. https://doi.org/10.1152/ajpheart.1981.240.3.H320

86. Takaoka H, Takeuchi M, Odake M, Yokoyama M (1992) Assessment of myocardial oxygen consumption (Vo2) and systolic pressure-volume area (PVA) in human hearts. European Heart Journal 13:85–90. https://doi.org/10.1093/eurheartj/13.suppl_E.85

87. Di Salvo TG, Mathier M, Semigran MJ, Dec GW (1995) Preserved right ventricular ejection fraction predicts exercise capacity and survival in advanced heart failure. Journal of the American College of Cardiology 25:1143–1153. https://doi.org/10.1016/0735-1097(94)00511-N

88. Vijiiac A, Onciul S, Guzu C, Scarlatescu A, Petre I, Zamfir D, Onut R, Deaconu S, Dorobantu M (2021) Forgotten No More—The Role of Right Ventricular Dysfunction in Heart Failure with Reduced Ejection Fraction: An Echocardiographic Perspective. Diagnostics 11:548. https://doi.org/10.3390/diagnostics11030548

89. Abouzeid CM, Shah T, Johri A, Weinsaft JW, Kim J (2017) Multimodality Imaging of the Right Ventricle. Curr Treat Options Cardio Med 19:82. https://doi.org/10.1007/s11936-017-0584-9

90. Todaro MC, Romano G, Carerj S, Clemenza F, Pilato M, Khandheria BK (2015) Right Ventricular Free Wall Strain: A Predictor of Successful Left Ventricular Assist Device Implantation. Texas Heart Institute Journal 42:87–89. https://doi.org/10.14503/THIJ-14-4111

91. Gumus F, Durdu MS, Cakici M, Kurklu TST, Inan MB, Dincer I, Sirlak M, Akar AR (2019) Right ventricular free wall longitudinal strain and stroke work index for predicting right heart failure after left ventricular assist device therapy. Interactive CardioVascular and Thoracic Surgery 28:674–682. https://doi.org/10.1093/icvts/ivy328

92. Dufendach KA, Zhu T, Diaz Castrillon C, Hong Y, Countouris ME, Hickey G, Keebler M, Thoma FW, Kilic A (2021) Pre-implant right ventricular free wall strain predicts post-LVAD right heart failure. J Card Surg 36:1996–2003. https://doi.org/10.1111/jocs.15479

93. Kovács A, Lakatos B, Tokodi M, Merkely B (2019) Right ventricular mechanical pattern in health and disease: beyond longitudinal shortening. Heart Fail Rev 24:511–520. https://doi.org/10.1007/s10741-019-09778-1

94. Contijoch FJ, Groves DW, Chen Z, Chen MY, McVeigh ER (2017) A novel method for evaluating regional RV function in the adult congenital heart with low-dose CT and SQUEEZ processing. International Journal of Cardiology 249:461–466. https://doi.org/10.1016/j.ijcard.2017.08.040

95. Pourmorteza A, Schuleri KH, Herzka DA, Lardo AC, McVeigh ER (2012) A New Method for Cardiac Computed Tomography Regional Function Assessment: Stretch Quantifier for Endocardial Engraved Zones (SQUEEZ). Circ Cardiovasc Imaging 5:243–250. https://doi.org/10.1161/CIRCIMAGING.111.970061

96. American Heart Association Writing Group on Myocardial Segmentation and Registration for Cardiac Imaging:, Cerqueira MD, Weissman NJ, Dilsizian V, Jacobs AK, Kaul S, Laskey WK, Pennell DJ, Rumberger JA, Ryan T, Verani MS (2002) Standardized Myocardial Segmentation and Nomenclature for Tomographic Imaging of the Heart: A Statement for Healthcare Professionals From the Cardiac Imaging Committee of the Council on Clinical Cardiology of the American Heart Association. Circulation 105:539–542. https://doi.org/10.1161/hc0402.102975

97. Kovacs G, Berghold A, Scheidl S, Olschewski H (2009) Pulmonary arterial pressure during rest and exercise in healthy subjects: a systematic review. European Respiratory Journal 34:888–894. https://doi.org/10.1183/09031936.00145608

98. Tadic M, Nita N, Schneider L, Kersten J, Buckert D, Gonska B, Scharnbeck D, Reichart C, Belyavskiy E, Cuspidi C, Rottbauer W (2021) The Predictive Value of Right Ventricular Longitudinal Strain in Pulmonary Hypertension, Heart Failure, and Valvular Diseases. Front Cardiovasc Med 8:698158. https://doi.org/10.3389/fcvm.2021.698158

99. Meng Y, Zhu S, Xie Y, Zhang Y, Qian M, Gao L, Li M, Lin Y, Wu W, Wang J, Yang Y, Lv Q, Zhang L, Li Y, Xie M (2021) Prognostic Value of Right Ventricular 3D Speckle-Tracking Strain and Ejection Fraction in Patients With HFpEF. Front Cardiovasc Med 8:694365. https://doi.org/10.3389/fcvm.2021.694365